CMS-HIG-12-035

arXiv:1303.0763v2 [hep-ex] 10 Jun 2013

Search for the standard model Higgs boson produced in association with a top-quark pair in pp collisions at the LHC

The CMS Collaboration[*]

Abstract

A search for the standard model Higgs boson produced in association with a top-quark pair is presented using data samples corresponding to an integrated luminosity of $5.0\,\mathrm{fb}^{-1}$ ($5.1\,\mathrm{fb}^{-1}$) collected in pp collisions at the center-of-mass energy of 7 TeV (8 TeV). Events are considered where the top-quark pair decays to either one lepton+jets ($t\bar{t} \to \ell\nu q\bar{q}'b\bar{b}$) or dileptons ($t\bar{t} \to \ell^+\nu\ell^-\bar{\nu}b\bar{b}$), ℓ being an electron or a muon. The search is optimized for the decay mode $H \to b\bar{b}$. The largest background to the $t\bar{t}H$ signal is top-quark pair production with additional jets. Artificial neural networks are used to discriminate between signal and background events. Combining the results from the 7 TeV and 8 TeV samples, the observed (expected) limit on the cross section for Higgs boson production in association with top-quark pairs for a Higgs boson mass of 125 GeV is 5.8 (5.2) times the standard model expectation.

Submitted to the Journal of High Energy Physics

[*]See Appendix A for the list of collaboration members

1 Introduction

With the recent observation [1, 2] at the Large Hadron Collider (LHC) of a new, Higgs-like particle with a mass of approximately 125 GeV, the focus of searches for the standard model (SM) Higgs boson has shifted to evaluating the consistency of this new particle with SM expectations. A key component in this effort will be to determine whether the new particle's observed couplings to other fundamental particles match the predictions for a SM Higgs boson. A deviation from expectations could provide hints of physics beyond the standard model.

In the SM, the dominant production mechanism for the Higgs boson at the LHC arises from gluon fusion, via the Higgs boson coupling to gluons through a heavy quark loop. However, with sufficient data, other production mechanisms, such as Higgs boson production via vector boson fusion or in association with a W boson, Z boson, or $t\bar{t}$ pair, should also be observable. Furthermore, there are a number of decay channels available to a SM Higgs boson with a mass of approximately 125 GeV. Although the dominant decay mode at this mass is to a pair of bottom quarks, decays to WW, ZZ, $\tau\tau$, and $\gamma\gamma$ are also experimentally accessible. The SM provides precise predictions for these production and decay rates that depend on the coupling strength of the Higgs boson to the other fundamental particles of the SM.

To date, the only combinations of production mechanism and decay mode that have been established at greater than three standard deviation (σ) significance for this newly observed particle are direct production, with the new particle decaying either to a pair of photons or a pair of W or Z bosons. In all three of these cases, the observed rates are in agreement with SM expectations for Higgs boson production within the experimental uncertainties. However, establishing the complete consistency of the couplings of this newly observed particle with SM expectations for the Higgs boson involves measuring the rate of production across all the various possible production and decay channels discussed above.

The analysis described herein focuses on the search for a Higgs boson produced in association with a pair of top quarks ($t\bar{t}H$ production) conducted at the Compact Muon Solenoid (CMS) experiment. The analysis considers Higgs boson masses between 110 and 140 GeV. The search is optimized for Higgs boson decays to a bottom-quark pair, but we do not exclude events from other Higgs boson decay modes. The rate at which this process occurs depends on the largest of the fermionic couplings to the Higgs boson, namely the couplings to the top and bottom quarks. These two key couplings will be particularly important in probing the new particle's consistency with SM expectations.

The $t\bar{t}H$ vertex is the most challenging one to probe directly. Measuring the rate of Higgs boson production through the gluon fusion process provides an indirect measurement of the coupling between the top quark and the Higgs boson because this production mechanism is dominated by a top-quark loop that couples the gluons to the Higgs boson [3]. Likewise, the decay of the Higgs boson to two photons receives a significant contribution from a top-quark loop, although the loop involving W bosons dominates in this process [4]. However, extraction of the coupling between the top quark and the Higgs boson in this way relies on the assumption that there are no new massive fundamental particles beyond those of the SM that contribute in the loop. Unless the Higgs boson is very heavy, it will not decay to top quarks. Therefore, for the mass range most favored for the SM Higgs [5], and for 125 GeV in particular, $t\bar{t}H$ production is the only way to probe the $t\bar{t}H$ vertex in a model-independent manner [6, 7].

In contrast, there are several processes that can be used to probe the coupling of this new particle to bottom quarks. Because of the large $b\bar{b}$ background from multijet production, it is not experimentally feasible to probe $H \to b\bar{b}$ in Higgs boson production via gluon fusion. Instead,

the search is typically made using associated production involving either a W or a Z boson (VH production). Although t̄tH production has a smaller expected cross section, this signature provides a probe that is complementary to the VH channel: they both provide information about the coupling between the bottom quark and the Higgs boson, but the dominant backgrounds are very different, t̄t + jets production instead of W + jets production.

An observation of t̄tH production, depending on the measured properties, might be consistent with the SM Higgs boson or could indicate something more exotic [8, 9]. Since the expected SM rates in this channel are very small, a sizeable excess would be clear evidence for new physics. A previous search at the Tevatron [10], the first such search conducted at a hadron collider, showed no significant excess over SM expectation.

This paper is organized as follows. Section 2 describes the CMS apparatus. Section 3 describes the data and simulation samples utilized in the analysis, while Section 4 discusses the object identification, event reconstruction and selection. The extraction of the t̄tH signal is discussed in Section 5, followed by a description of the impact of systematic uncertainties encountered in the analysis in Section 6. The results of this search are reported in Section 7 and followed by a summary in Section 8.

2   The CMS detector

The CMS detector consists of the following main components. A superconducting solenoid occupies the central region of the CMS detector, providing an axial magnetic field of 3.8 T parallel to the beam direction. The silicon pixel and strip tracker, the crystal electromagnetic calorimeter and the brass/scintillator hadron calorimeter are located in concentric layers within the solenoid. These layers provide coverage out to $|\eta| = 2.5$, where pseudorapidity is defined as $\eta = -\ln\left[\tan\left(\theta/2\right)\right]$. A quartz-fiber Cherenkov hadron forward calorimeter extends further to $|\eta| < 5.2$. The CMS experiment uses a right-handed coordinate system, with the origin at the nominal interaction point, the x axis pointing to the center of the LHC ring, the y axis pointing up (perpendicular to the LHC plane), and the z axis along the counterclockwise beam direction. The polar angle θ is measured from the positive z axis and the azimuthal angle ϕ is measured in the x-y plane in radians. Muons are detected by gas-ionization detectors embedded in the steel flux return yoke outside the solenoid. The first level of the CMS trigger system, composed of custom hardware processors, is designed to select the most interesting events in less than $3\,\mu$s using information from the calorimeters and muon detectors. The high-level trigger processor farm further decreases the event rate to a few hundred Hz for data storage. More details about the CMS detector can be found in Ref. [11].

3   Data and simulation samples

This search is performed with samples of proton-proton collisions at $\sqrt{s} = 7\,\text{TeV}$ and $8\,\text{TeV}$, collected with the CMS detector in 2011 and 2012, respectively. These data correspond to a total integrated luminosity of $5.0\,\text{fb}^{-1}$ at $7\,\text{TeV}$ and $5.1\,\text{fb}^{-1}$ at $8\,\text{TeV}$.

All background and signal processes are modeled using Monte Carlo (MC) simulations from MADGRAPH 5.1.1 [12], PYTHIA 6.4.24 [13], and POWHEG 1.0 [14] event generators, depending on the physics process. The MC samples use CTEQ6L1 [15] parton distribution functions (PDFs) of the proton, except for the POWHEG samples, which use CTEQ6M. The t̄tH signal events are generated using PYTHIA. The main background t̄t sample is generated with MADGRAPH, with matrix elements corresponding to up to three additional partons which are then

matched to parton showers produced by PYTHIA. The additional partons generated with the t$\bar{\text{t}}$ sample include b and c quarks in addition to light flavored quarks and gluons. Decays of τ leptons are handled with TAUOLA 2.75 [16]. MADGRAPH is also used to simulate t$\bar{\text{t}}$W, t$\bar{\text{t}}$Z, W + jets, and Drell–Yan (DY) processes, with up to 4 partons in the final state. The DY contribution includes all Z/$\gamma^* \to \ell\ell$ processes with the dilepton invariant mass $m_{\ell\ell} > 10\,\text{GeV}$. Single-top production is modeled with the next-to-leading order (NLO) generator POWHEG combined with PYTHIA. Electroweak diboson processes (WW, WZ, and ZZ) are simulated using PYTHIA.

All background and signal process rates are estimated using NLO or higher theoretical predictions. The t$\bar{\text{t}}$H cross section [17–24] and Higgs branching fractions [25–28] used in the analysis have NLO accuracy. The t$\bar{\text{t}}$ and diboson cross sections are calculated at NLO with MCFM [29–31]. The single-top-quark production rates are normalized to an approximately next-to-next-to-leading order (NNLO) calculation [32–35]. The W+jets and DY+jets rates are normalized to inclusive NNLO cross sections from FEWZ [36, 37]. The t$\bar{\text{t}}$W and t$\bar{\text{t}}$Z rates are normalized to the NLO predictions from Refs. [38, 39]. These cross sections are allowed to vary within their uncertainties in the fit we use to calculate the limit.

Effects from additional pp interactions in the same bunch crossing (pileup) are modeled by adding simulated minimum-bias events (generated with PYTHIA) to the simulated processes. The CMS detector response is simulated using the GEANT4 software package [40]. The pileup multiplicity distribution in MC is reweighted to reflect the luminosity profile of the observed pp collisions. We apply an additional correction factor to account for residual differences in the jet transverse momentum (p_T) spectrum due to pileup; the event-by-event correction factor is based on the difference between simulation and data in the distribution of the scalar sum of the transverse momenta of the jets in the event. We include a systematic shape uncertainty in association with this correction factor. In addition to correcting the MC due to pileup, we also apply jet energy resolution corrections [41] and lepton and trigger efficiency scale factors to the MC events.

4   Event reconstruction and selection

This analysis selects events consistent with the production of a Higgs boson in association with a top-quark pair (see Fig. 1). In the SM, the top quark is expected to decay to a W boson and a bottom quark nearly 100% of the time. Hence different t$\bar{\text{t}}$ decay modes can be identified according to the subsequent decays of the W bosons. Here we consider two t$\bar{\text{t}}$ decay modes: the lepton+jets mode (t$\bar{\text{t}} \to \ell\nu\text{q}\bar{\text{q}}'\text{b}\bar{\text{b}}$), where one W boson decays leptonically, and the dilepton mode (t$\bar{\text{t}} \to \ell^+\nu\ell^-\bar{\nu}\text{b}\bar{\text{b}}$), where both W bosons do so. For the lepton+jets case, we select events containing an energetic, isolated, electron or muon, and at least four energetic jets, two or more of which should be identified as originating from a b quark (b-tagged) [42]. For the dilepton case, we require a pair of oppositely charged energetic leptons (two electrons, two muons, or one electron and one muon) and two or more jets, with at least two of the jets being b-tagged.

Object reconstruction is based on the particle flow (PF) algorithm [43], which combines the information from all CMS subdetectors to identify and reconstruct individual objects including muons, electrons, photons, and charged and neutral hadrons produced in an event. To minimize the impact of pileup, charged particles are required to originate from the primary vertex, which is identified as the reconstructed vertex with the largest value of Σp_T^2, where the summation includes all tracks associated with that vertex. In both channels, a significant amount of missing transverse energy (E_T^miss) should be present due to the presence of neutrinos, however no explicit requirement on the E_T^miss is used in the event selection. The E_T^miss vector is calculated as the negative of the vectorial sum of the transverse momenta of all particles. For both chan-
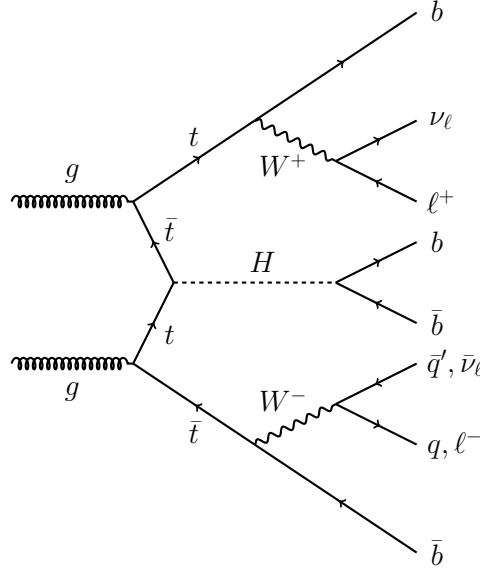
Figure 1: A leading-order Feynman diagram for t$\bar{\text{t}}$H production, illustrating the two top-quark pair system decay channels considered here, and the H $\to$ b$\bar{\text{b}}$ decay mode for which the analysis is optimized.

nels, we use a common set of criteria for selecting individual objects (electrons, muons, and jets) which is described below.

In the lepton+jets channel, the data were recorded with triggers requiring the presence of either a single muon or electron. The trigger muon candidate was required to be isolated from other activity in the event and to have $p_\text{T} > 24\,\text{GeV}$ for both the 2011 and 2012 data-taking periods. In 2011, the trigger electron candidate was required to have transverse energy $E_\text{T} > 25\,\text{GeV}$ and to be produced in association with at least three jets with $p_\text{T} > 30\,\text{GeV}$, whereas in 2012, a single-electron trigger with minimum E_T threshold of 27 GeV was used. In the dilepton channel, the data were recorded with triggers requiring any combination of electrons and muons, one lepton with $p_\text{T} > 17\,\text{GeV}$ and another with $p_\text{T} > 8\,\text{GeV}$. The offline object selection detailed below is designed to select events in the plateau of the trigger efficiency turn-on curve.

Muons are reconstructed using information from the tracking detectors and the muon chambers [44]. Tight muons must satisfy additional quality criteria based on the number of hits associated with the muon candidate in the pixel, strip, and muon detectors. For lepton+jets events, tight muons are required to have $p_\text{T} > 30\,\text{GeV}$ and $|\eta| < 2.1$ to ensure the full trigger efficiency. For dilepton events, tight muons are required to have $p_\text{T} > 20\,\text{GeV}$ and $|\eta| < 2.1$. Loose muons in both channels are required to have $p_\text{T} > 10\,\text{GeV}$ and $|\eta| < 2.4$. The muon isolation is assessed by calculating the scalar sum of the p_T of charged particles from the same primary vertex and neutral particles in a cone of $\Delta R = \sqrt{(\Delta\eta)^2 + (\Delta\phi)^2} = 0.4$ around the muon direction, excluding the muon itself; the resulting sum is corrected for the effects of neutral hadrons from pileup interactions. The ratio of this corrected isolation sum to the muon p_T is the relative isolation of the muon. For tight muons, the relative isolation is required to be less than 0.12. For loose muons, this ratio must be less than 0.2.

Electrons are reconstructed using both calorimeter and tracking information [45]. Any electron that can be paired with an oppositely charged particle consistent with the conversion of an energetic photon is rejected. Tight electrons in lepton+jets events are required to have

$E_T > 30\,\text{GeV}$, while in dilepton events they must have $E_T > 20\,\text{GeV}$. Loose electrons must have $E_T > 10\,\text{GeV}$. All electrons are required to have $|\eta| < 2.5$. Electrons that fall into the transition region between the barrel and endcap of the electromagnetic calorimeter ($1.442 < |\eta| < 1.566$) are rejected because the reconstruction of an electron object in this region is not optimal. The isolation for electrons is calculated in a similar manner to muon isolation; however, for electrons the isolation sum is calculated in a cone of $\Delta R = 0.3$. In the same way as for muons, the relative isolation is the ratio of this corrected isolation sum to the electron E_T. Tight electrons must have a relative isolation less than 0.1, while loose electrons must have a relative isolation less than 0.2.

In both channels of this search, all events are required to contain at least one tight lepton, either a muon or an electron. The second lepton in the dilepton channel may be loose or tight, while in the lepton+jets channel events with a second loose lepton are rejected to ensure the same events do not enter both channels.

Jets are reconstructed by clustering the charged and neutral PF particles using the anti-k_T algorithm with a distance parameter of 0.5 [46, 47]. Particles identified as isolated muons and electrons are expected to come from W decays and are excluded from the clustering. Non-isolated muons and electrons are expected to come from b-decays and are included in the clustering. The momentum of a jet is determined from the vector sum of all particle momenta in the jet candidate and is scaled according to jet energy corrections, based on simulation, jet plus photon data events and dijet data events [41]. Charged PF particles not associated with the primary event vertex are ignored when reconstructing jets. The neutral component coming from pileup events is removed by applying a residual energy correction following the area-based procedure described in Refs. [48, 49]. In the lepton+jets channel, we require at least three jets with $p_T > 40\,\text{GeV}$ and a fourth jet with $p_T > 30\,\text{GeV}$. In the dilepton analysis, we require at least two jets with $p_T > 30\,\text{GeV}$. All jets must have a pseudorapidity in the range $|\eta| < 2.4$.

Jets are identified as originating from a b quark using the combined secondary vertex (CSV) algorithm [42]. This algorithm combines information about the impact parameter of tracks and reconstructed secondary vertices within the jets in a multivariate algorithm designed to separate jets containing the decay products of bottom-flavored hadrons from jets originating from charm quarks, light quarks, or gluons. The CSV algorithm provides a continuous output discriminant; high values of the CSV discriminant indicate that the jet is more consistent with being a b jet, while low values indicate the jet is more likely a light-quark jet. To select b-tagged jets, a selection is placed on the CSV discriminant distribution such that the efficiency is 70% (20%) for jets originating from a b (c) quark and the probability of tagging jets originating from light quarks or gluons is 2%. In addition, the CSV discriminant values for the selected jets are used in the signal extraction as described in Section 5. For MC events, the CSV discriminant values of each jet are adjusted so that the proportion of b jets, c jets, and light-quark jets of different η and p_T values passing each of three CSV working points (tight, medium, and loose) is the same in data and MC. The adjustment factor is computed using a linear interpolation between CSV working points.

Figure 2 shows the jet and b-tagged jet multiplicities for events selected in the lepton+jets channel. For both lepton+jets and dilepton channels, signal t$\bar{\text{t}}$H events are generally characterized by having more jets and more tags than the background processes. To increase the sensitivity of this analysis, we separate the selected events into different categories based on the number of jets and tags. For lepton+jets events, we use the following seven categories: ≥ 6 jets + 2 b-tags, 4 jets + 3 b-tags, 5 jets + 3 b-tags, ≥ 6 jets + 3 b-tags, 4 jets + 4 b-tags, 5 jets + ≥ 4 b-tags, and ≥ 6 jets + ≥ 4 b-tags. For dilepton events, only two categories are used: 2 jets + 2 b-tags and ≥ 3 jets +

≥3 b-tags. Tables 1–3 show the predicted signal, background, and observed yields in each category for the lepton+jets and dilepton channels. Background estimates are obtained from MC after the appropriate corrections and scale factors have been applied, as described above. Given the event selection criteria and the large jet and b-tag multiplicity requirements in the lepton+jets channel, the background from QCD multijet production is negligible. Uncertainties in signal and background yields include both statistical and systematic sources. Sources of systematic uncertainty are described in Section 6. In Tables 1–3, the $t\bar{t}$ + jets background is separated into the $t\bar{t}$ + $b\bar{b}$, $t\bar{t}$ + $c\bar{c}$, and $t\bar{t}$+light flavor (lf) components. The categories with higher jet and tag multiplicities are the most sensitive to signal. We include less sensitive categories in order to better constrain the background.

The choice of event selection categories outlined above is optimized for the H → $b\bar{b}$ decay mode. However, in the higher end of our search range—including m_H = 125 GeV—other decay modes, especially WW and $\tau\tau$, can have significant standard model branching fractions. For the purposes of this search, we define any $t\bar{t}$H event as signal, regardless of the Higgs boson decay. For most of the event selection categories defined above, the contribution from the decay modes other than H → $b\bar{b}$ is less than 10%. The largest contribution from the non-$b\bar{b}$ decay modes arises in the ≥6 jets + 2 b-tags lepton+jets category where almost 50% of the events come from decay modes other than H → $b\bar{b}$. In that category H → WW dominates the non-$b\bar{b}$ contribution. With the current optimization, the impact of the non-$b\bar{b}$ decay modes to the analysis sensitivity is negligible as the contribution from H → $b\bar{b}$ in the most sensitive categories is > 95%.

5 Signal extraction

Artificial neural networks (ANNs) [50] are used in all categories of the analysis to further discriminate signal from background and improve signal sensitivity. Separate ANNs are trained for each jet-tag category, and the choice of input variables is optimized for each as well. The ANN input variables considered are related to object kinematics, event shape, and the discriminant output from the b-tagging algorithm. A total of 24 input variables has been considered and are listed in column 1 of Table 4. The inputs are selected from a ranked list based on initial separation between signal and background. The separation of the individual variables is evaluated using a separation benchmark $\langle S^2 \rangle$ [51] defined as follows:

$$\langle S^2 \rangle = \frac{1}{2} \int \frac{(\hat{y}_S(y) - \hat{y}_B(y))^2}{\hat{y}_S(y) + \hat{y}_B(y)} \mathrm{d}y, \tag{1}$$

where y is the input variable, and $\hat{y}_S$ and $\hat{y}_B$ are the signal and background probability density functions for that input variable in the signal and background samples, respectively. The maximum number of input variables considered is determined by the statistics in the simulated samples used for ANN training. The number of variables per category is determined by reducing the number of variables until the minimum number of variables needed to maintain roughly the same ANN performance is reached. In the lepton+jets categories, the use of approximately 10 input variables yields stable performance; using fewer inputs exhibits degraded discrimination power, and using more inputs exhibits little improvement in performance in most categories. A similar exercise was done for the dilepton categories. The choice of input variables for each jet-tag category used in the 8 TeV analysis is summarized in Table 4; the input variables for each category in the 7 TeV analysis are very similar. The input variables used in the ANN can be broken down into several classes, as detailed below.
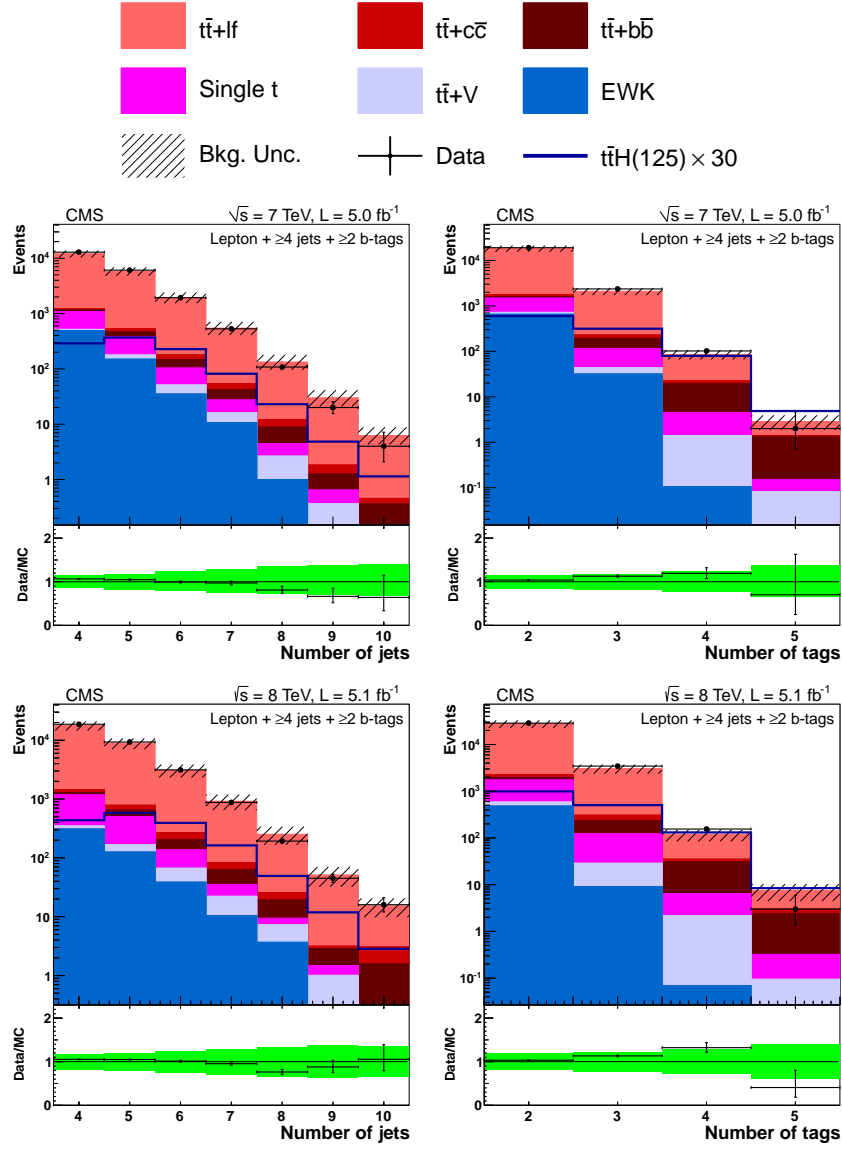
Figure 2: Number of jets (left) and number of b-tagged jets (right) in data and simulation for events with ≥4 jets + ≥2 b-tags in the lepton+jets channel at 7 TeV (top) and 8 TeV (bottom). The background is normalized to the SM expectation; the uncertainty band (shown as a hatched band in the stack plot and a green band in the ratio plot) includes statistical and systematic uncertainties that affect both the rate and shape of the background distributions. The $t\bar{t}H$ signal ($m_H = 125$ GeV) is normalized to $30 \times$ SM expectation.

Table 1: Expected event yields for backgrounds (bkg), signal, and number of observed events in the lepton+jets channel in 7 TeV data.

	≥6 jets 2 b-tags	4 jets 3 b-tags	5 jets 3 b-tags	≥6 jets 3 b-tags	4 jets 4 b-tags	5 jets ≥4 b-tags	≥6 jets ≥4 b-tags
$t\bar{t}H(125)$	6.1 ± 0.9	2.7 ± 1.1	4.0 ± 1.6	3.8 ± 1.6	0.4 ± 0.2	1.1 ± 0.4	1.4 ± 0.6
$t\bar{t}$+lf	2040 ± 520	940 ± 170	590 ± 120	346 ± 92	15.7 ± 3.3	22.8 ± 5.3	26.1 ± 7.7
$t\bar{t} + b\bar{b}$	31 ± 17	26 ± 13	28 ± 15	24 ± 13	2.1 ± 1.1	5.7 ± 3.1	8.4 ± 4.8
$t\bar{t} + c\bar{c}$	37.5 ± 9.5	10.1 ± 1.9	12.8 ± 2.7	11.8 ± 3.2	0.5 ± 0.1	1.0 ± 0.3	1.5 ± 0.5
$t\bar{t}$ V	18.4 ± 3.5	3.2 ± 0.6	4.3 ± 0.8	4.5 ± 0.9	0.2 ± 0.0	0.5 ± 0.1	0.7 ± 0.2
Single t	54.8 ± 7.0	40.0 ± 5.1	21.8 ± 3.3	9.6 ± 1.6	1.2 ± 0.4	1.0 ± 0.3	0.8 ± 0.3
V+jets	41 ± 26	21 ± 11	4.9 ± 4.8	0.5 ± 0.6	0.0 ± 0.0	0.0 ± 0.0	0.1 ± 0.1
Diboson	0.6 ± 0.2	0.7 ± 0.2	0.7 ± 0.2	0.3 ± 0.2	0.0 ± 0.0	0.0 ± 0.0	0.0 ± 0.0
Total bkg	2230 ± 540	1040 ± 180	660 ± 130	396 ± 99	19.7 ± 4.1	30.9 ± 7.3	38 ± 11
Data	2137	1214	736	413	18	37	49

Table 2: Expected event yields for backgrounds (bkg), signal, and number of observed events in the lepton+jets channel in 8 TeV data.

	≥6 jets 2 b-tags	4 jets 3 b-tags	5 jets 3 b-tags	≥6 jets 3 b-tags	4 jets 4 b-tags	5 jets ≥4 b-tags	≥6 jets ≥4 b-tags
$t\bar{t}H(125)$	11.7 ± 1.9	3.9 ± 1.8	6.1 ± 2.8	6.9 ± 3.1	0.6 ± 0.3	1.5 ± 0.7	2.5 ± 1.2
$t\bar{t}$+lf	3460 ± 940	1320 ± 280	870 ± 210	570 ± 170	18.0 ± 5.1	27.6 ± 8.6	41 ± 15
$t\bar{t} + b\bar{b}$	61 ± 34	35 ± 19	43 ± 24	35 ± 20	2.5 ± 1.7	8.4 ± 5.3	15.4 ± 9.4
$t\bar{t} + c\bar{c}$	62 ± 17	19.6 ± 5.1	25.0 ± 6.9	25.9 ± 7.7	0.6 ± 0.4	0.8 ± 0.9	3.7 ± 1.8
$t\bar{t}$ V	35.7 ± 7.5	4.5 ± 1.1	6.1 ± 1.4	8.6 ± 2.1	0.1 ± 0.1	0.7 ± 0.2	1.5 ± 0.4
Single t	79 ± 18	56 ± 11	25.6 ± 6.2	10.3 ± 2.9	0.3 ± 0.6	3.1 ± 2.2	1.0 ± 0.6
V+jets	53 ± 40	5.9 ± 6.0	0.8 ± 0.9	0.0 ± 0.0	0.0 ± 0.0	0.0 ± 0.0	0.0 ± 0.0
Diboson	1.2 ± 0.4	1.8 ± 0.6	0.5 ± 0.2	0.2 ± 0.1	0.0 ± 0.0	0.0 ± 0.0	0.0 ± 0.0
Total bkg	3760 ± 980	1440 ± 300	970 ± 230	650 ± 190	21.5 ± 6.1	41 ± 12	63 ± 21
Data	3503	1646	1116	686	28	56	74

Table 3: Expected event yields for backgrounds (bkg), signal, and number of observed events in the dilepton channel in 7 TeV and 8 TeV data.

	7 TeV Data		8 TeV Data	
	2 jets + 2 b-tags	≥3 jets + ≥3 b-tags	2 jets + 2 b-tags	≥3 jets + ≥3 b-tags
$t\bar{t}H(125)$	0.5 ± 0.2	2.1 ± 0.9	0.7 ± 0.3	3.3 ± 1.5
$t\bar{t}$+lf	3280 ± 590	109 ± 25	4100 ± 780	135 ± 34
$t\bar{t} + b\bar{b}$	6.5 ± 3.4	16.1 ± 8.6	7.6 ± 4.2	25 ± 14
$t\bar{t} + c\bar{c}$	5.1 ± 1.0	7.5 ± 1.8	10.1 ± 2.8	14.1 ± 4.1
$t\bar{t}$ V	2.6 ± 0.5	2.3 ± 0.5	3.5 ± 0.8	3.8 ± 0.9
Single t	99 ± 11	3.9 ± 0.8	129 ± 18	6.2 ± 2.4
V+jets	810 ± 190	23.5 ± 9.7	830 ± 200	29 ± 13
Diboson	25.8 ± 2.7	0.6 ± 0.1	29.2 ± 3.7	0.7 ± 0.2
Total bkg	4230 ± 660	163 ± 35	5110 ± 860	215 ± 48
Data	4303	185	5406	251

Table 4: The ANN inputs for the nine jet-tag categories in the 8 TeV $t\bar{t}H$ analysis in the lepton+jets and dilepton channels. The choice of inputs is optimized for each category. Definitions of the variables are given in the text. The best input variable for each jet-tag category is denoted by ★.

	Lepton+Jets							Dilepton	
Jets	≥ 6	4	5	≥ 6	4	5	≥ 6	2	≥ 3
Tags	2	3	3	3	4	≥ 4	≥ 4	2	≥ 3
Jet 1 p_T		✓	✓		✓			★	✓
Jet 2 p_T		✓	✓						
Jet 3 p_T	✓	✓	✓			✓			
Jet 4 p_T	✓	✓	✓			✓			
N_jets									✓
$p_\mathrm{T}(\ell, E_\mathrm{T}^\mathrm{miss}, \mathrm{jets})$		★	✓		✓	✓		✓	✓
$M(\ell, E_\mathrm{T}^\mathrm{miss}, \mathrm{jets})$	✓	✓		✓	✓		✓		
Average $M((\mathrm{j}_m^\mathrm{untag}, \mathrm{j}_n^\mathrm{untag}))$	✓			✓					
$M((\mathrm{j}_m^\mathrm{tag}, \mathrm{j}_n^\mathrm{tag})_\mathrm{closest})$							✓		
$M((\mathrm{j}_m^\mathrm{tag}, \mathrm{j}_n^\mathrm{tag})_\mathrm{best})$							✓		
Average $\Delta R(\mathrm{j}_m^\mathrm{tag}, \mathrm{j}_n^\mathrm{tag})$				✓	✓	✓	✓		
Minimum $\Delta R(\mathrm{j}_m^\mathrm{tag}, \mathrm{j}_n^\mathrm{tag})$			✓					✓	✓
$\Delta R(\ell, \mathrm{j}_\mathrm{closest})$						✓	✓	✓	✓
Sphericity	✓			✓			✓		
Aplanarity	✓				✓				
H_0	✓								
H_1	✓				✓				
H_2				✓			✓		
H_3	★			✓			✓		
μ^CSV	✓	✓	★	★	★	★	★	✓	★
$(\sigma_n^\mathrm{CSV})^2$		✓	✓	✓	✓	✓			
Highest CSV value						✓			
2nd-highest CSV value		✓	✓	✓	✓	✓	✓		
Lowest CSV value		✓	✓	✓	✓	✓	✓		

The first class of variables are those that are basic kinematic properties of single objects in the event or combinations of objects. These variables include the p_T of the leading four jets, and the p_T and mass of the system defined by the vector sum of the lepton(s) momenta, the E_T^{miss} vector, and the momenta of the jets in the event ($p_T(\ell, E_T^{miss}, \text{jets})$ and $M(\ell, E_T^{miss}, \text{jets})$, respectively), all of which favor larger values for $t\bar{t}H$ signal than for the backgrounds. The number of jets is used in the ≥ 3 jets + ≥ 3 b-tags category in the dilepton analysis since $t\bar{t}H$ signal favors larger jet multiplicity than background.

A related class of variables involves looking at the kinematic properties of pairs of jets. The H $\to$ b$\bar{b}$ decay produces jets that have a large invariant mass even if the jets fail the b-tag selection. Other untagged jets in the event tend to come from hadronic W decay and initial- or final-state radiation, and tend to have a small invariant mass compared to the jets from the Higgs boson decay. For this reason, some signal discrimination is provided by examining the invariant mass of pairs of untagged jets in lepton+jets categories with six or more jets but fewer than four b-tagged jets.

Likewise, the 6-jet category with four or more tags uses two variables that rely specifically on the H $\to$ b$\bar{b}$ hypothesis: the invariant mass of the tagged-jet pair with the smallest opening angle ($M((j_m^{tag}, j_n^{tag})_{closest})$), and the "best Higgs mass" ($M((j_m^{tag}, j_n^{tag})_{best})$), the invariant mass constructed from the two tagged jets least likely to be a part of the $t\bar{t}$ system as determined by a minimum χ^2 search among all the jet, lepton, and E_T^{miss} combinations in the event, using the W and top masses as kinematic constraints. The $M((j_m^{tag}, j_n^{tag})_{closest})$ distribution for both signal and background has a peak near the same value; however, the distribution is wider in the case of signal, offering some discriminating power. In signal events, the "best Higgs mass" is highly correlated with the Higgs boson mass. Although the peak is broadened by events where the wrong jets are associated with the Higgs boson decay, this variable still provides some power in discriminating signal from background. The ≥ 6 jets + ≥ 4 b-tags uses 11 variables instead of the typical 10 because it was shown that the addition of the "best Higgs mass" variable, uniquely designed for this jet-tag category, offers a non-negligible increase in expected ANN performance.

Another class of variables exploits differences in the "shape" of events between signal and background. In general, production of an extra massive object, in addition to top quarks tends to make $t\bar{t}H$ events more spherical in shape, while the background events are more collimated or have more jet activity. Variables in this class include angular correlations, like the opening angle between the tagged jets ($\Delta R(j_m^{tag}, j_n^{tag})$) or between the lepton and closest jet ($\Delta R(\ell, j_{closest})$), where in the dilepton analysis the angle is calculated with respect to the lepton leading in p_T. More complex event shape variables like sphericity and aplanarity [52], as well as the Fox–Wolfram moments H_0, H_1, H_2, H_3 [53], also exhibit differences between signal and background.

The last class of variables used in the ANN involves the CSV discriminant values of the tagged jets. The signal events tend to have more b jets than the dominant $t\bar{t}$ + jets background. Beyond the simple multiplicity of tagged jets we can, however, exploit the overall b-jet content of the signal in several ways. For instance, the average and squared-deviation from this average of the CSV discriminant values for the tagged jets (μ^{CSV}, $(\sigma_n^{CSV})^2$ for the n-th tagged jet) are powerful variables. Events with genuine b jets will have higher average CSV discriminant values and the b jets themselves will have CSV values more tightly clustered around high values than those from light-flavour or charm jets which are tagged.

Using the procedure discussed above, different variables are chosen for use in each of the different event selection categories. This is motivated by the fact that although the $t\bar{t}$+jets background is dominant throughout, the kinematics of the events can be very distinct in different

jet multiplicity bins. Similarly, the tagging discriminant of the b jets clearly is different in events with 2, 3 or $\geq$4 b-tags. Finally, the overall breakdown of the t$\bar{\text{t}}$+jets background into t$\bar{\text{t}}$ + b$\bar{\text{b}}$, t$\bar{\text{t}}$ + c$\bar{\text{c}}$ and t$\bar{\text{t}}$+light-flavor is different across the jet-tag categories, implying different variables will be more effective in some categories than others.

In nearly all event selection categories, the variables that discriminate best between signal and background directly involve b-tagging information, such as the average CSV output value for b-tagged jets. This is natural, since the largest fraction of the backgrounds in all categories involve events with fewer b jets than the t$\bar{\text{t}}$H generally has. However, when considering specifically the t$\bar{\text{t}}$ + b$\bar{\text{b}}$, a background very similar to the signal, the b-tagging information alone is not as powerful, and additional information from kinematic variables and angular correlations, such as the minimum ΔR between all pairs of b-tagged jets, become important. Even so, the t$\bar{\text{t}}$ + b$\bar{\text{b}}$ background remains difficult to separate from the t$\bar{\text{t}}$H signal.

Figures 3 through 5 show the variables used in the ANN for the 5 jets + 3 b-tags category (lepton+jets channel) and the 2 jets + 2 b-tags (dilepton channel). The 5 jets + 3 b-tags category is chosen for lepton+jets as a compromise between signal sensitivity and adequate statistics for display purposes. Also shown, in Figure 6, are data-to-simulation comparisons of the best input variables for each jet-tag category considered in the 8 TeV analysis. The data-to-simulation ratio plots in Figures 3 through 6 show that, within uncertainties, the simulation reproduces well the shape and normalization of the distributions of the variables used in the ANN before the final maximum likelihood fit is performed (as discussed in Section 7). Correlations between input variables are also well reproduced by simulation.

For ANN training, we use t$\bar{\text{t}}$H (m_{H} = 120 GeV) as the signal and t$\bar{\text{t}}$+jets as the background, such that there is an equal amount of both for each category. The mass m_{H} = 120 GeV sample was chosen in the analysis of the 7 TeV data before the observation of a Higgs-like particle at m_{H} = 125 GeV was announced. This mass point was preserved in the 8 TeV ANN training for consistency. The signal and background events used to train an ANN are split in half: one half is used to do the training itself, while the other is used as an independent test sample to monitor performance during training. The ANN method used is the "multilayer perceptron", available as part of the TMVA [51] package in ROOT [54]. A multilayer perceptron is a specific kind of neural network in which the neurons in each layer only have connections to neurons in the following layer. The network architecture used here consists of two hidden layers, with N neurons in the first layer and $N - 1$ neurons in the second layer, where N is the number of input variables. Standard tests were completed during ANN training to look for evidence of overtraining; no such evidence was found in any jet-tag category, providing confidence that our training statistics were satisfactory given the number of input variables used in each.

The ANN output provides better discrimination between signal and background than any one of the input variables individually. Figures 7 and 8 show the ANN output for all the categories of the lepton+jets channel in 7 TeV and 8 TeV data, respectively, and Figs. 9 and 10 show output distributions for dilepton events. We use these ANN output distributions for the signal extraction as described in Section 7.

6 Systematic uncertainties

Table 5 lists the systematic uncertainties that affect signal and background yields, the shape of the ANN output, or both. The effects of these uncertainties are evaluated specifically for each event selection category, and the effects from the same source are treated as completely correlated across the categories. The impact on the rate is the relative change in expected yield
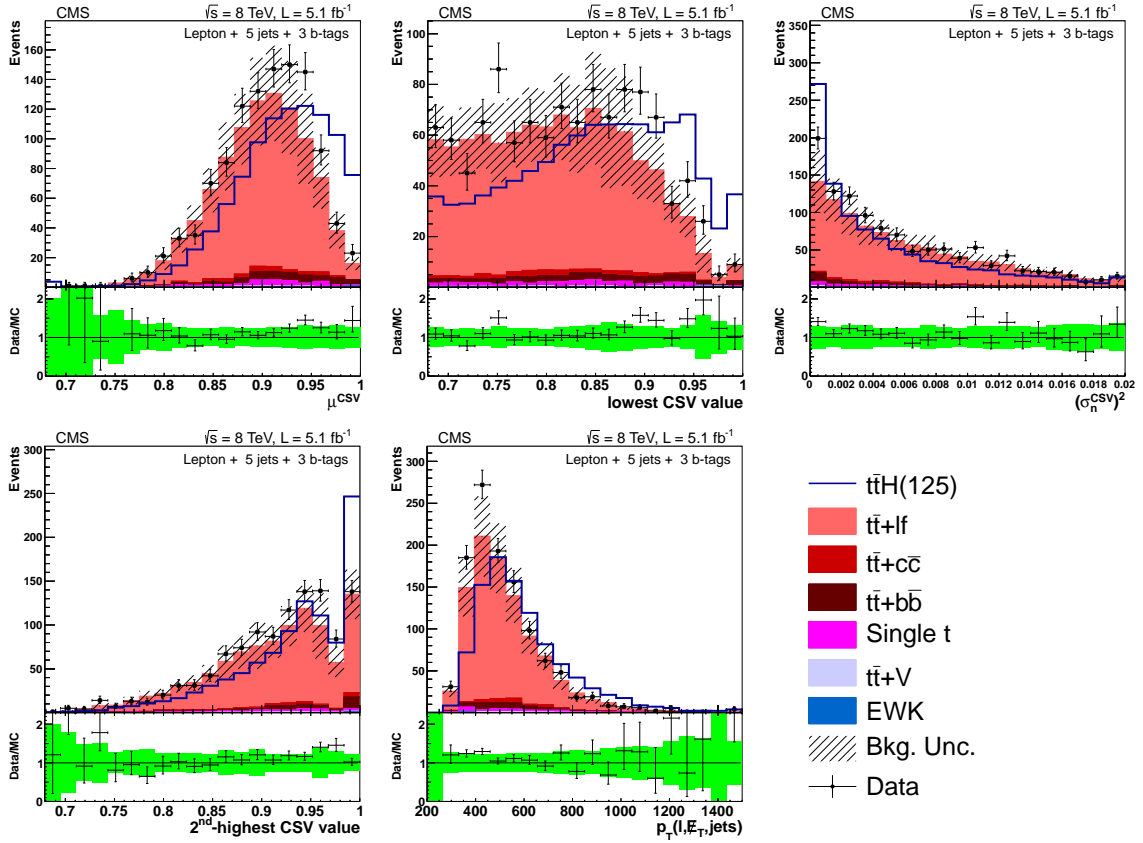
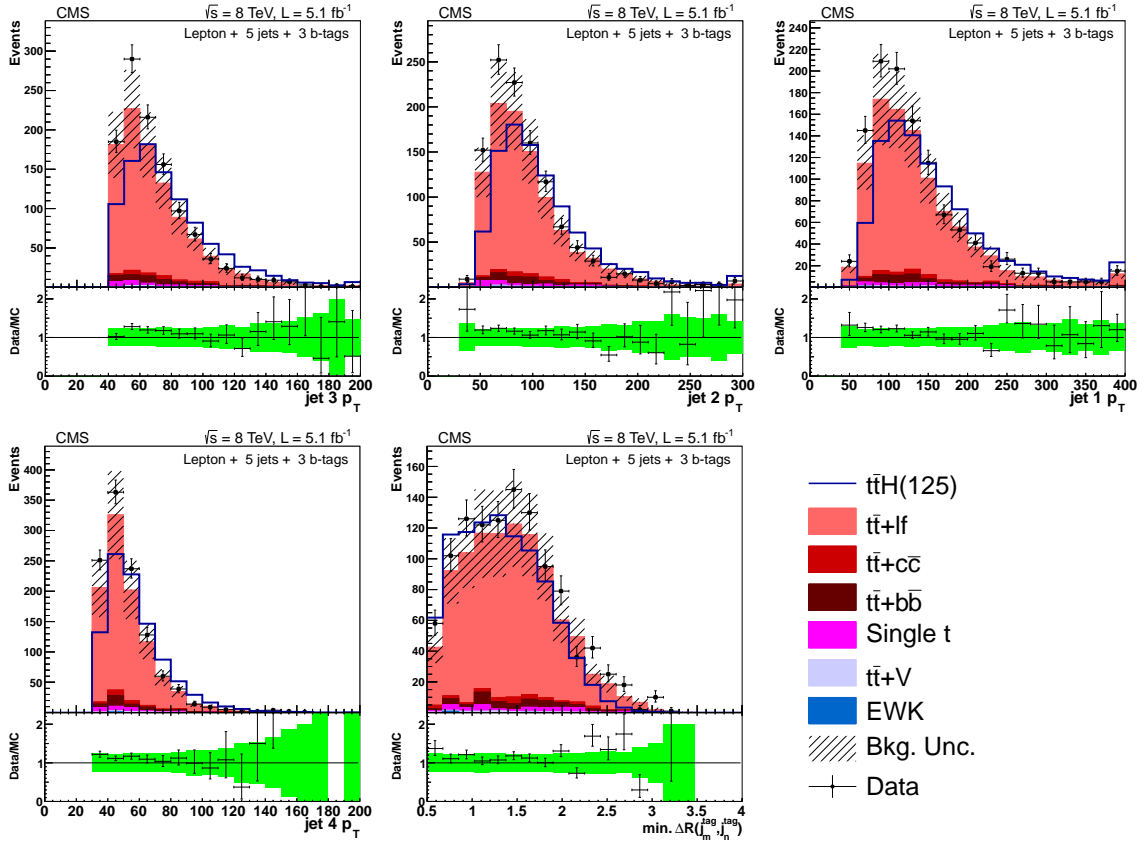Figure 3: Distributions of the five ANN input variables with rankings 1 through 5, in terms of separation, for the 5 jets + 3 b-tags category of the lepton+jets channel at 8 TeV. Definitions of the variables are given in the text. The background is normalized to the SM expectation; the uncertainty band (shown as a hatched band in the stack plot and a green band in the ratio plot) includes statistical and systematic uncertainties that affect both the rate and shape of the background distributions. The $t\bar{t}H$ signal ($m_H = 125$ GeV) is normalized to $\sim 150 \times$ SM expectation, equal to the total background yield, for easier comparison of the shapes.

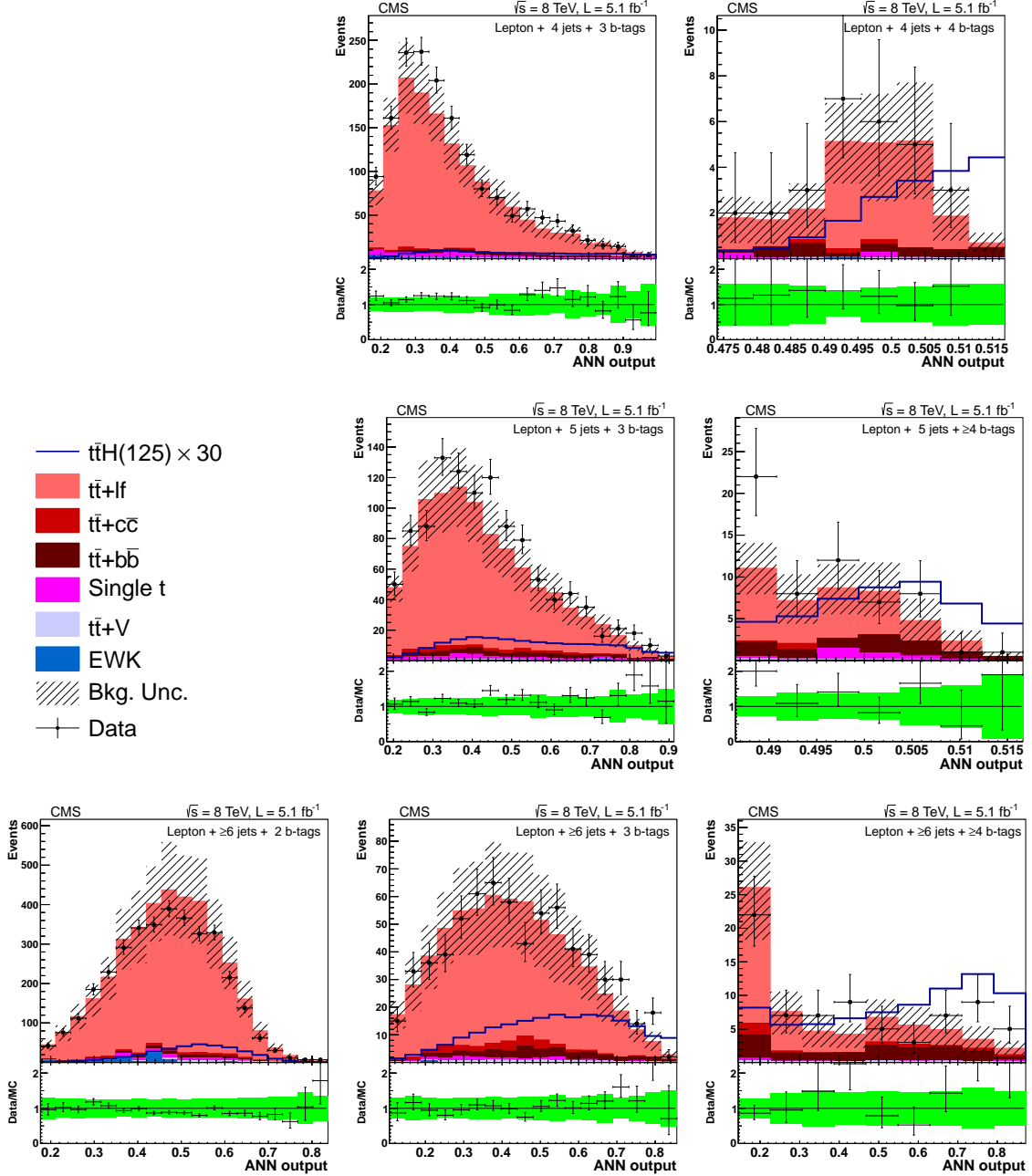Figure 4: Distributions of the five ANN input variables with rankings 6 through 10, in terms of separation, for the 5 jets + 3 b-tags category of the lepton+jets channel at 8 TeV. Definitions of the variables are given in the text. The background is normalized to the SM expectation; the uncertainty band (shown as a hatched band in the stack plot and a green band in the ratio plot) includes statistical and systematic uncertainties that affect both the rate and shape of the background distributions. The t̄tH signal ($m_H = 125\,\text{GeV}$) is normalized to ∼150 × SM expectation, equal to the total background yield, for easier comparison of the shapes.
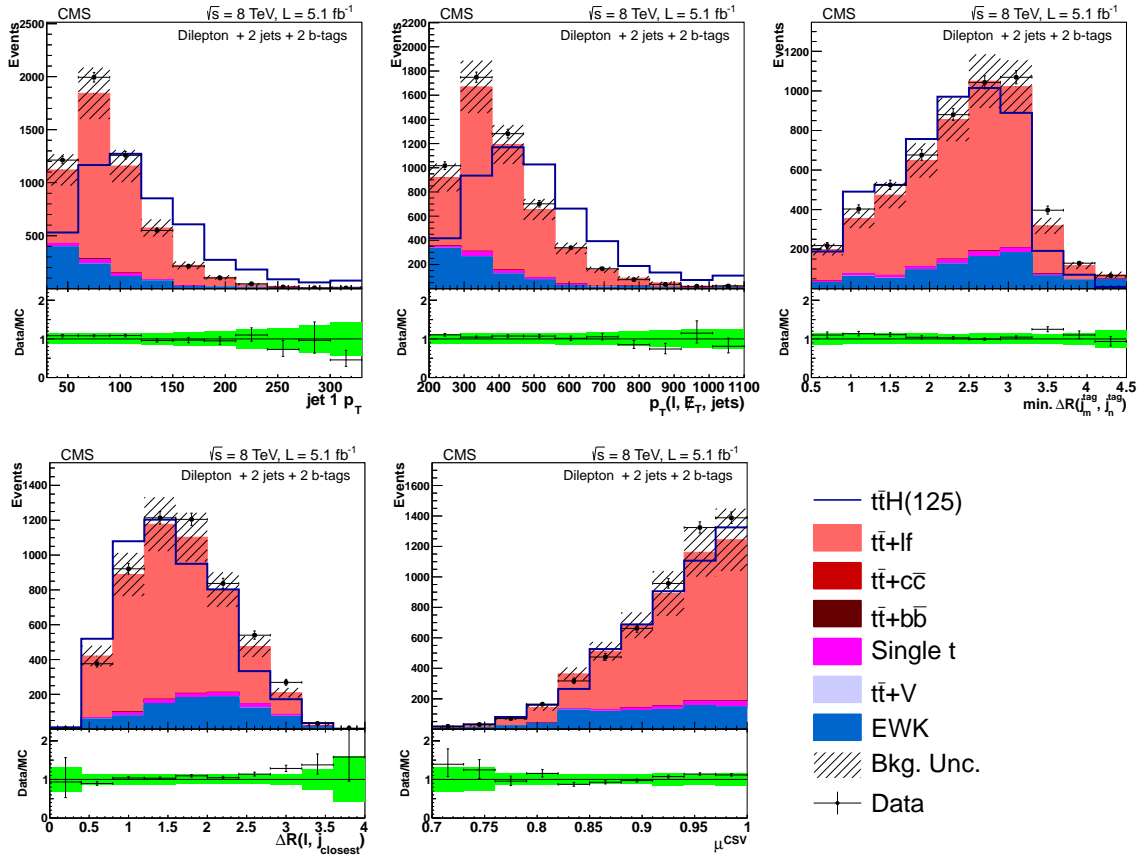
Figure 5: Distributions of ANN input variables for the 2 jets + 2 b-tags category of the dilepton channel at 8 TeV. Definitions of the variables are given in the text. The background is normalized to the SM expectation; the uncertainty band (shown as a hatched band in the stack plot and a green band in the ratio plot) includes statistical and systematic uncertainties that affect both the rate and shape of the background distributions. The $t\bar{t}H$ signal ($m_H = 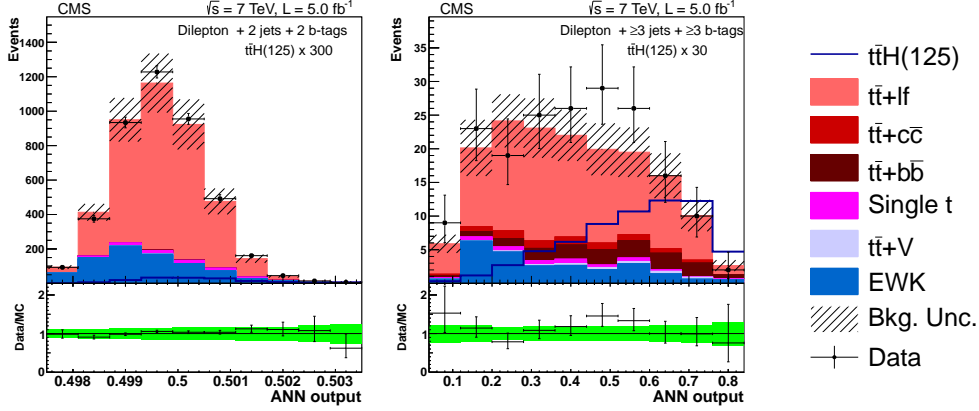125$ GeV) is normalized to $\sim7000 \times$ SM expectation, equal to the total background yield, for easier comparison of the shapes.
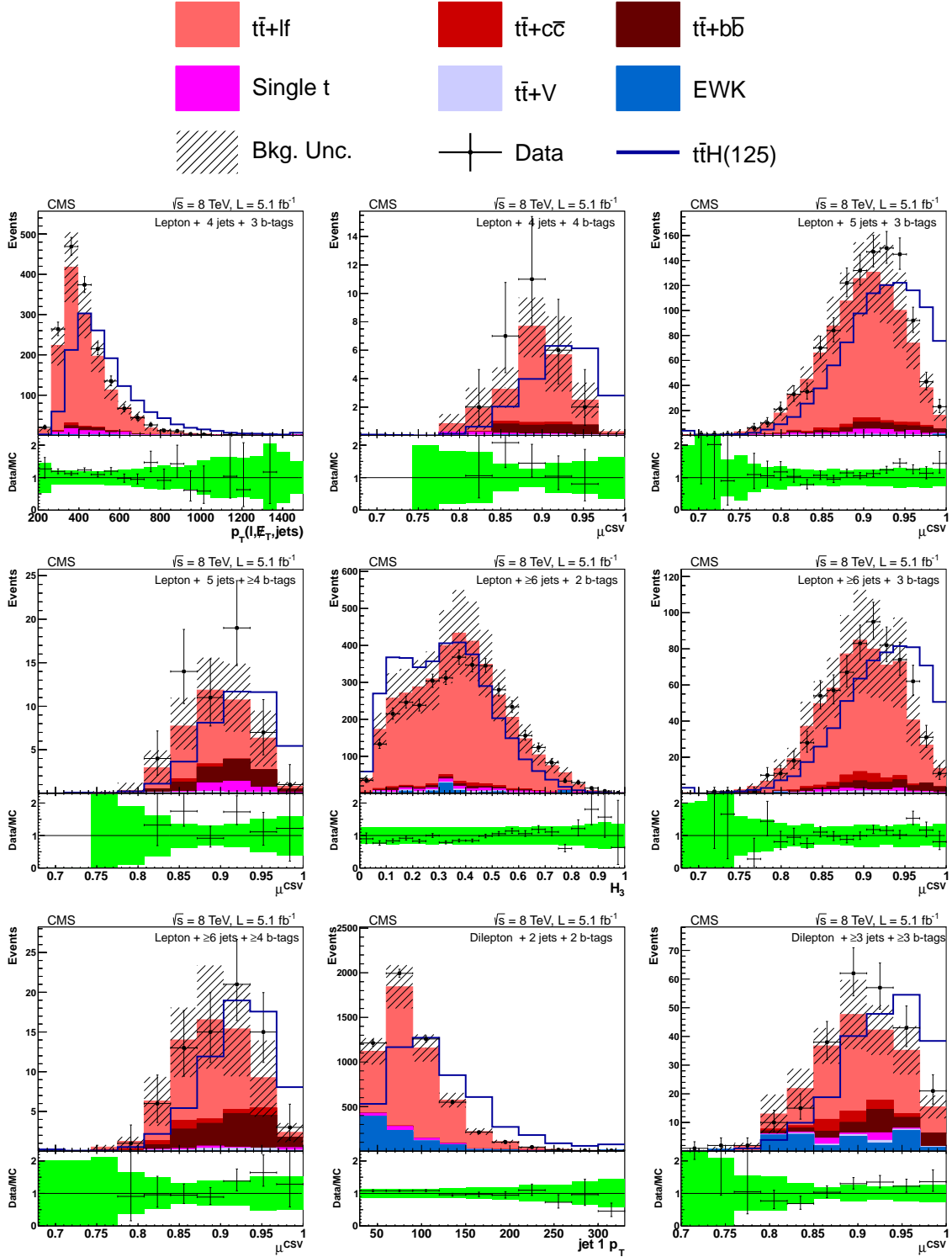
Figure 6: Input variables that give the best signal-background separation power for each of the lepton + jets and dilepton jet, b-tag categories used in the analysis at 8 TeV. Definitions of the variables are given in the text. The background is normalized to the SM expectation; the uncertainty band (shown as a hatched band in the stack plot and a green band in the ratio plot) includes statistical and systematic uncertainties that affect both the rate and shape of the background distributions. The t$\bar{\text{t}}$H signal ($m_{\text{H}} = 125$ GeV) is normalized to $\sim$25–7000 $\times$ SM expectation, equal to the total background yield for that category, for easier comparison of the shapes.
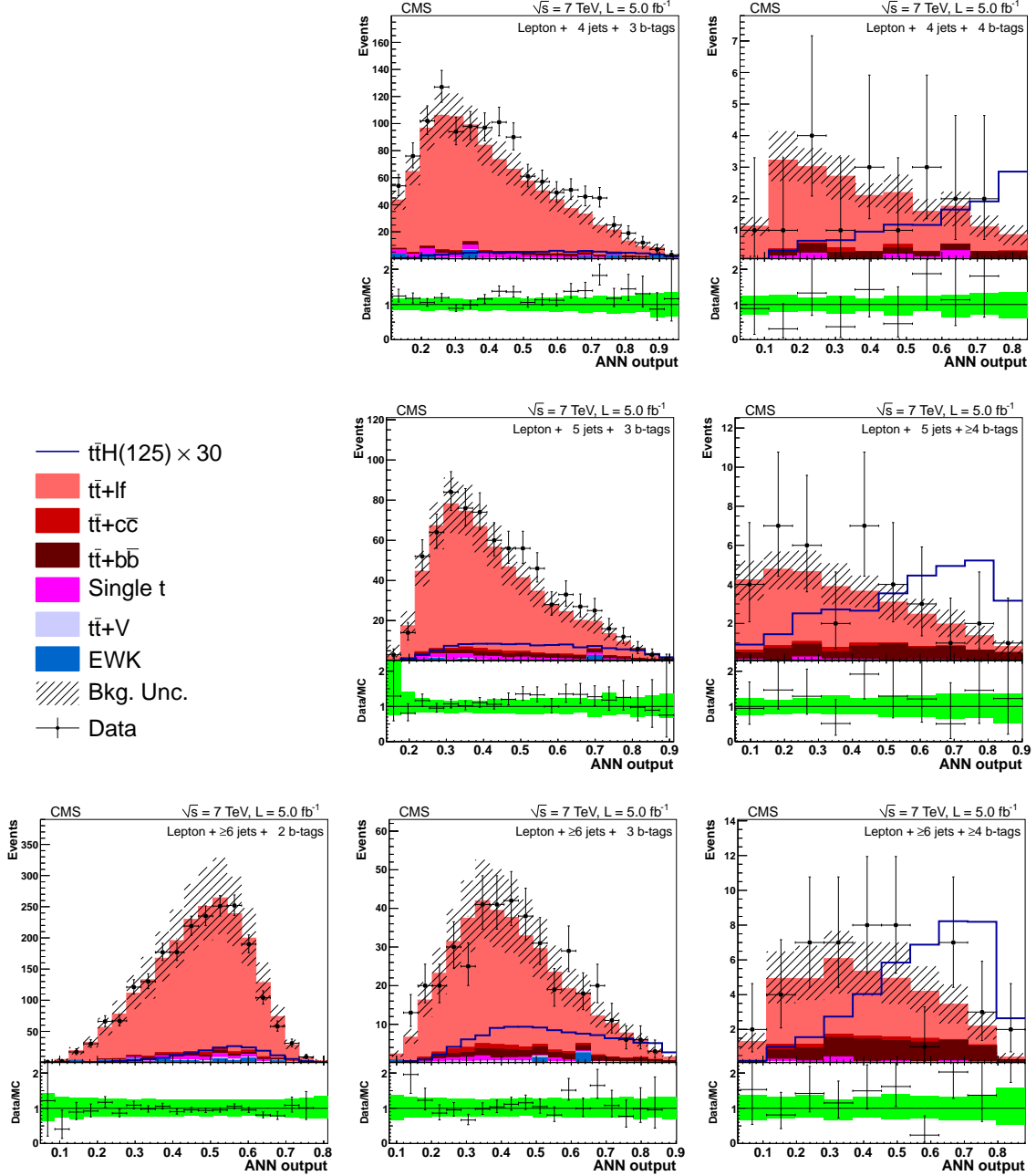
Figure 7: The distributions of the ANN output for lepton+jets events at 7 TeV in the various analysis categories. The top, middle, and bottom rows are events with 4, 5, and ≥6 jets, respectively, while the left, middle, and right-hand columns are events with 2, 3, and ≥4 b-tags, respectively. Background-like events have a low ANN output value. Signal-like events have a high ANN output value. The background is normalized to the SM expectation; the uncertainty band (shown as a hatched band in the stack plot and a green band in the ratio plot) includes statistical and systematic uncertainties that affect both the rate and shape of the background distributions. The t$\bar{\text{t}}$H signal ($m_H = 125$ GeV) is normalized to 30 × SM expectation.

Figure 8: The distributions of the ANN output for lepton+jets events at 8 TeV in the various analysis categories. The top, middle and, bottom rows are events with 4, 5, and ≥6 jets, respectively, while the left, middle, and right-hand columns are events with 2, 3, and ≥4 b-tags, respectively. Background-like events have a low ANN output value. Signal-like events have a high ANN output value. The background is normalized to the SM expectation; the uncertainty (shown as a hatched band in the stack plot and a green band in the ratio plot) includes statistical and systematic uncertainties that affect both the rate and shape of the background distributions. The tt̄H signal ($m_H = 125$ GeV) is normalized to $30 \times$ SM expectation.

Figure 9: The distributions of the ANN output for dilepton events at 7 TeV in the various analysis categories. The left plot shows events with 2 jets + 2 b-tags and right plot shows events with $\geq$3 jets + $\geq$3 b-tags. The background is normalized to the SM expectation; the uncertainty (shown as a hatched band in the stack plot and a green band in the ratio plot) band includes statistical and systematic uncertainties that affect both the rate and shape of the background distributions. The tt̄H signal ($m_H = 125$ GeV) is normalized to 300 or 30 × SM expectation for the 2 jets + 2 b-tags and the $\geq$3 jets + $\geq$3 b-tags categories, respectively.
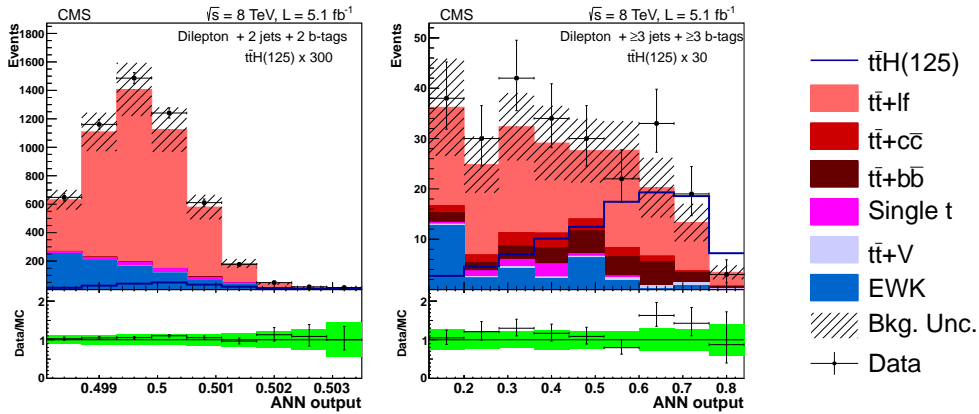
Figure 10: The distributions of the ANN output for dilepton events at 8 TeV in the various analysis categories. The left plot shows events with 2 jets + 2 b-tags and right plot shows events with $\geq$3 jets + $\geq$3 b-tags. The background is normalized to the SM expectation; the uncertainty (shown as a hatched band in the stack plot and a green band in the ratio plot) includes statistical and systematic uncertainties that affect both the rate and shape of the background distributions. The tt̄H signal ($m_H = 125$ GeV) is normalized to 300 or 30 × SM expectation for the 2 jets + 2 b-tags and the $\geq$3 jets + $\geq$3 b-tags categories, respectively.

due to each uncertainty. Some sources of uncertainty affect predicted yields for all processes in each category uniformly, while in some cases the uncertainty affects the predicted yield of some processes in certain categories more than others; in the latter cases the range of the effect on the predicted yield is given across all processes in all categories. Hence large relative rate changes listed in Table 5 can typically be attributed to processes with small expected yields in a single category that change significantly when considering a source of uncertainty.

Table 5: Summary of the systematic uncertainties considered on the inputs to the limit calculation. Except where noted, each row in this table will be treated as a single, independent nuisance parameter.

Source	Rate Uncertainty	Shape	Remarks
Luminosity (7 TeV)	2.2%	No	All signal and backgrounds
Luminosity (8 TeV)	4.4%	No	All signal and backgrounds
Lepton ID/Trig	4%	No	All signal and backgrounds
Pileup	1%	No	All signal and backgrounds
Additional Pileup Corr.	–	Yes	All signal and backgrounds
Jet Energy Resolution	1.5%	No	All signal and backgrounds
Jet Energy Scale	0–60%	Yes	All signal and backgrounds
b-Tag SF (b/c)	0–33.6%	Yes	All signal and backgrounds
b-Tag SF (mistag)	0–23.5%	Yes	All signal and backgrounds
MC Statistics	–	Yes	All backgrounds
PDF (gg)	9%	No	For gg initiated processes ($t\bar{t}$, $t\bar{t}Z$, $t\bar{t}H$)
PDF (q$\bar{q}$)	4.2–7%	No	For q$\bar{q}$ initiated processes ($t\bar{t}W$, W, Z).
PDF (qg)	4.6%	No	For qg initiated processes (single top)
QCD Scale ($t\bar{t}H$)	15%	No	For NLO $t\bar{t}H$ prediction
QCD Scale ($t\bar{t}$)	2–12%	No	For NLO $t\bar{t}$ and single top predictions
QCD Scale (V)	1.2–1.3%	No	For NNLO W and Z prediction
QCD Scale (VV)	3.5%	No	For NLO diboson prediction
Madgraph Scale ($t\bar{t}$)	0–20%	Yes	$t\bar{t}$ + jets/$b\bar{b}$/$c\bar{c}$ uncorrelated. Varies by jet bin.
Madgraph Scale (V)	20–60%	No	Varies by jet bin.
$t\bar{t}$ + $b\bar{b}$	50%	No	Only $t\bar{t}$ + $b\bar{b}$.

Lepton identification and trigger efficiency uncertainties were found to have a small impact on the analysis. The uncertainties were estimated by comparing variations in the difference in performance between data and MC simulation using a high-purity sample of Z-boson decays. The largest variations were at most 4% for a small fraction of events, such as electrons at low p_T. The analysis conservatively uses 4% uncertainty on the lepton scale overall. To ascertain the effects of the uncertainty on the pileup distribution, the cross section used to predict the distribution of pileup interactions in MC is varied by 8% from its nominal value, and the resulting change in the number of pileup interactions is propagated through the analysis. The systematic uncertainty due to the additional pileup correction, based on the scalar sum of the p_T of the jets, is evaluated by doubling or removing the correction applied. The uncertainty on the luminosity estimate corresponding to the 7 TeV dataset is 2.2% [55] and, for the 8 TeV dataset, 4.4% [56].

The uncertainty from the jet energy scale [41] is evaluated by varying the energy scale for all jets in the signal and background predictions up and down by one standard deviation as a function of jet p_T and η and re-evaluating the yields and ANN shapes of all processes. Similarly, the uncertainty on the jet energy resolution is obtained by varying the jet energy resolution correction up and down by one standard deviation, although in this case the effect on shape is negligible and therefore not included.

The b-tagging scale factor corrects the b-tagging efficiency in simulation to match that mea-

sured in data [42]. The uncertainty on this scale factor is evaluated by varying it up and down by one standard deviation and the new CSV output value corresponding to that uncertainty is recalculated. This new CSV value is used to determine both the number of tags associated with that systematic and the new shape of variables that use the CSV output, such as the average CSV value for b-tagged jets. This uncertainty affects both rate and shape estimates. Since the b-tagging scale factor uncertainty affects the ANN shape differently for events with different number of jets or number of b-tagged jets, we conservatively assume no correlations among all the categories.

We account for the effect of background MC statistics in our analysis using the approach described in [57, 58]. To make the limit computation more efficient and stable, we do not evaluate this uncertainty for any bin in the ANN shapes for which the MC statistical uncertainty is negligible compared to the data statistics or where there is no appreciable contribution from signal. In total, there are 64 nuisance parameters used to describe the MC statistics for the 8 TeV results, but only five are needed for 7 TeV, due to the larger MC statistics available for those samples. Tests show that the effect of neglecting bins as described above is smaller than 5%.

Theoretical uncertainties on the cross sections used to predict the rates of various processes are propagated to the yield estimates. All rates are estimated using cross sections of at least NLO accuracy, which have uncertainties arising primarily from PDFs and the choice of factorization and renormalization scales. The cross section uncertainties are each separated into their PDF and scale components and correlated where appropriate between processes. For example, the PDF uncertainty for processes originating primarily from gluon-gluon initial states, e.g., $t\bar{t}$ and $t\bar{t}H$ production, are treated as 100% correlated.

In addition, for the $t\bar{t} + \text{jets}$ (including $t\bar{t} + b\bar{b}$ and $t\bar{t} + c\bar{c}$) and the V+jets processes, the inclusive NLO or better cross section prediction are extrapolated to exclusive rates for particular jet or tag categories using the MADGRAPH tree-level matrix element generator matched to the PYTHIA parton shower MC program. Although MADGRAPH incorporates contributions from higher-order diagrams, because it does so only at tree-level, it is subject to fairly large uncertainties arising from the choice of scale. These uncertainties are evaluated using samples for which the factorization and renormalization scales have been varied up and down by a factor of two. The rate uncertainty arising from this source varies with the number of additional jets in the production diagram, and is larger for events with more jets. The effect of scale variations on the ANN output shape is also included for the $t\bar{t} + \text{jets}$ sample. Scale variations are treated as uncorrelated for the $t\bar{t}+\text{light flavour}$, $t\bar{t} + b\bar{b}$, and $t\bar{t} + c\bar{c}$ components to cover the uncertainty in the relative yields of those processes; the impact on the ANN output shape from scale variation in the V+jets processes is neglected, since this contribution is small in most categories. The scale variations for $W + \text{jets}$ and $Z + \text{jets}$ are treated as correlated with each other, but uncorrelated with $t\bar{t} + \text{jets}$.

As the background due to the $t\bar{t} + b\bar{b}$ contribution is very similar to the signal, the uncertainty on its rate and shape will have a substantial impact on our search. Due to the lack of more accurate higher order theoretical predictions for this process, we estimated this background and assessed its uncertainty based on the inclusive $t\bar{t}$ sample and the most important contribution to the uncertainty comes from the factorization and renormalization scale systematics. Neither control region studies nor higher-order theoretical calculations [59] can currently constrain the normalization of the $t\bar{t} + b\bar{b}$ contribution to better than 50% accuracy. Therefore, to be conservative, an extra 50% rate uncertainty is assigned to $t\bar{t} + b\bar{b}$ for both 7 TeV and 8 TeV.

7 Results

A maximum likelihood fit is performed on the ANN output distributions from the nine jet-tag categories considered in the analysis. We consider the model including the SM backgrounds and a Higgs boson signal, as well as a model with only SM backgrounds but no Higgs boson signal. As we currently lack sensitivity to detect a SM Higgs boson signal, and observe no significant excess in the data, we focus here on setting 95% confidence level (CL) upper limits on the possible presence of a SM-like signal.

The statistical methodology employed by this analysis is identical to that used for other CMS searches [2, 60, 61]. In brief, we use a modified frequentist CL_s [62, 63] approach in which the test statistic involves the ratio of the likelihood functions constructed from the background expectations plus the SM Higgs boson signal scaled by an arbitrary parameter μ, where $\mu \geq 0$. The parameter $\mu = \sigma/\sigma_{SM}$ is the ratio of the cross section of our signal process (σ) to the expected SM Higgs boson cross section (σ_{SM}). The likelihood function describes the expected yield of signal and background in bins of the ANN output for each event selection category. The systematic uncertainties described in Section 6 are incorporated into the likelihood by means of nuisance parameters that affect each background's rate, shape or both. Shape variations are handled by means of template morphing. A vertical template morphing approach is used where the shapes are smoothly interpolated between the $\pm 1\sigma$ varied shapes and linearly extrapolated outside that region. This is the standard template morphing approach used by all CMS Higgs analyses. As appropriate for the frequentist approach taken here, the nuisance parameters are profiled during the limit extraction. The nuisance parameter correlations are implemented in a way that accounts for event migrations between the selection categories. Furthermore, in cases involving shape systematics, where high-statistics, background-rich categories might overconstrain certain systematic effects in the lower-statistics, higher-sensitivity categories, we take the approach of decorrelating the nuisance parameters to avoid overly aggressive constraints.

When combining the results from the 7 TeV and 8 TeV datasets, the proper correlation in systematic effects must be represented in the nuisance parameter choices. Given that for all theoretical predictions and many experimental uncertainties, exactly the same calculation or calibration is applied to the 7 TeV and 8 TeV datasets, the associated systematic uncertainties are treated as completely correlated and a single nuisance parameter is used to implement the effect. There are two exceptions to this approach. The luminosity is evaluated separately for the two analyses and the dominant uncertainties are largely independent, so the luminosity uncertainty is treated as uncorrelated between 7 TeV and 8 TeV. Furthermore, as separate MC samples are used for the two datasets, the MC statistical uncertainties are treated as uncorrelated between the two datasets.

Background-dominated categories are used to constrain the fitted background contributions in the signal-enhanced categories. The prediction from the fit for the composition of the selected sample in each category more accurately describes the data than the prediction directly from simulation, and the uncertainties on the final composition are reduced. The resulting distributions are driven by the shape from $t\bar{t}$+light flavor, the dominant background in each category. No significant excesses of data above the background-only predictions are observed, and we use our statistical treatment to extract upper limits on the amount of $t\bar{t}H$ production consistent with our data. Figure 11 shows the 95% CL upper limit on the ratio μ of the $t\bar{t}H$ cross section with respect to that predicted by the SM as a function of m_H for the 7 TeV and 8 TeV samples, separately, combining both lepton+jets and dilepton channels in each dataset. Figure 12 shows the upper limit obtained by combining both data samples. Table 6 shows the expected and

observed limits for 7 TeV, 8 TeV, and combined analysis, using both the lepton+jets and the dilepton channels. The expected limit is extracted from the background-only hypothesis with no Higgs signal present. In addition to the median expected limit, the bands that contain 68% (1 standard deviation) and 95% (2 standard deviations) around the median are also quoted. The median expected limit for a Higgs boson mass of 125 GeV is $5.2 \times \sigma_{SM}$ while the observed limit is $5.8 \times \sigma_{SM}$.

As a cross check, we extracted the limit using the best single variable according to Table 4 and plotted in Fig. 6 instead of the ANN output. Otherwise, the analysis was performed in exactly the same way as the version based on the ANN, including the event selection categories, systematic uncertainties, and treatment of the nuisance parameters. The resulting median expected limit, for a Higgs boson mass of 125 GeV is $6.6 \times \sigma_{SM}$, approximately 27% higher than the limit obtained with the ANN. The primary reason for this decrease in sensitivity is the loss of separating power and the increased susceptibility to individual systematic effects coming from using fewer variables. The observed limit obtained using the best single variable analysis is $10.4 \times \sigma_{SM}$, which is beyond the 68% CL range (on μ) of the expected ($[5.0, 9.2]$) but within the 95% CL range ($[4.0, 12.7]$).

Table 6: Observed and expected 95% CL upper limits on $\mu = \sigma / \sigma_{SM}$ for the SM Higgs boson in the lepton+jets and dilepton channels combined, using the 7 TeV dataset, 8 TeV dataset, and both datasets combined.

7 TeV Lepton+Jets and Dilepton				
			Expected	
m_H	Observed	Median	68% CL Range	95% CL Range
110 GeV	4.1	4.4	[3.3, 6.3]	[2.7, 8.7]
115 GeV	4.7	5.0	[3.7, 7.1]	[2.9, 10.0]
120 GeV	5.5	5.8	[4.3, 8.2]	[3.4, 11.4]
125 GeV	6.2	6.9	[5.2, 9.7]	[4.1, 13.6]
130 GeV	7.3	8.8	[6.5, 12.5]	[5.0, 17.3]
135 GeV	8.8	10.8	[7.9, 15.4]	[6.3, 21.3]
140 GeV	10.4	14.2	[10.2, 20.0]	[8.2, 27.8]

8 TeV Lepton+Jets and Dilepton				
			Expected	
m_H	Observed	Median	68% CL Range	95% CL Range
110 GeV	5.6	3.3	[2.4, 4.7]	[2.0, 6.9]
115 GeV	6.6	4.1	[3.0, 5.8]	[2.5, 8.1]
120 GeV	8.2	5.1	[3.8, 7.1]	[3.1, 10.0]
125 GeV	8.7	5.7	[4.3, 8.2]	[3.5, 11.3]
130 GeV	10.4	6.9	[5.2, 9.8]	[4.2, 13.9]
135 GeV	13.7	9.4	[7.1, 13.1]	[5.7, 18.3]
140 GeV	15.2	11.3	[8.5, 16.2]	[6.8, 22.5]

7 TeV + 8 TeV Lepton+Jets and Dilepton combined				
			Expected	
m_H	Observed	Median	68% CL Range	95% CL Range
110 GeV	4.0	3.2	[2.4, 4.6]	[1.8, 6.5]
115 GeV	4.5	3.8	[2.8, 5.4]	[2.2, 7.5]
120 GeV	5.5	4.5	[3.3, 6.4]	[2.7, 8.9]
125 GeV	5.8	5.2	[3.7, 7.3]	[2.9, 10.1]
130 GeV	6.8	6.5	[4.8, 9.2]	[3.6, 12.9]
135 GeV	8.3	8.4	[6.1, 11.9]	[4.8, 16.3]
140 GeV	8.6	10.4	[7.5, 14.9]	[5.9, 20.5]
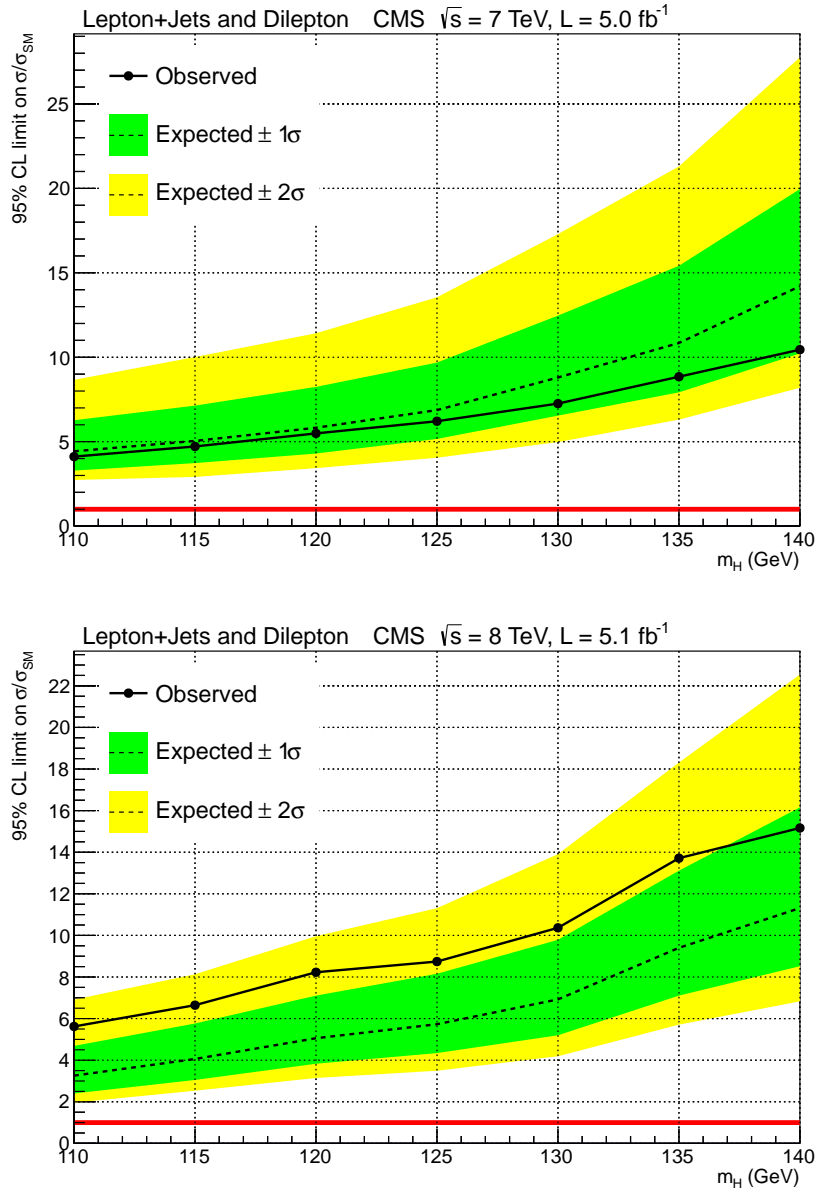
Figure 11: The observed and expected 95% CL upper limits on the signal strength parameter $\mu = \sigma/\sigma_{\mathrm{SM}}$ for lepton+jets and dilepton channels combined using the 2011 dataset at 7 TeV (above) and the 2012 dataset at 8 TeV (below).
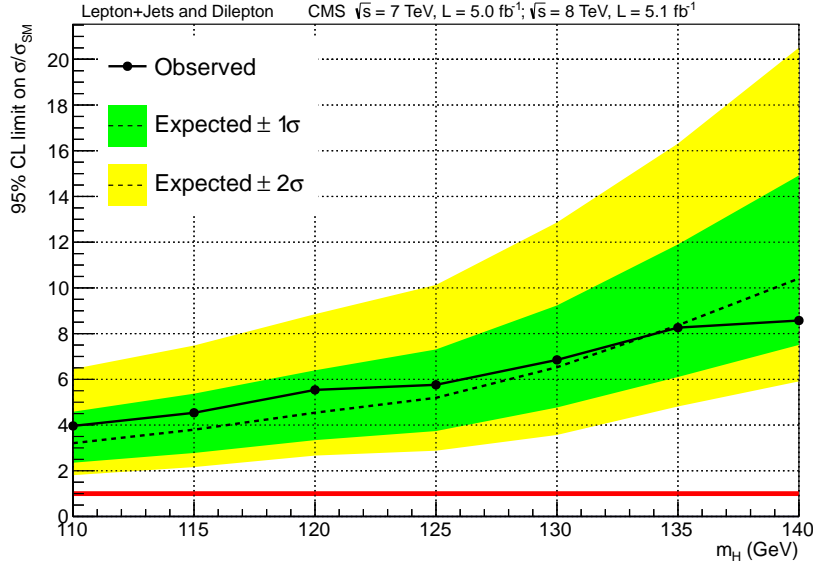
Figure 12: Using the 2011+2012 datasets, the observed and expected 95% CL upper limits on the signal strength parameter $\mu = \sigma/\sigma_{SM}$ for lepton+jets and dilepton channels combined.

8 Summary

A search for the standard model Higgs boson produced in association with a top-quark pair has been performed at the CMS experiment using data samples corresponding to an integrated luminosity of $5.0\,\mathrm{fb}^{-1}$ ($5.1\,\mathrm{fb}^{-1}$) collected in pp collisions at the center-of-mass energy of 7 TeV (8 TeV). Events are considered where the top-quark pair decays to either one lepton+jets ($t\bar{t} \rightarrow \ell\nu q\bar{q}'b\bar{b}$) or dileptons ($t\bar{t} \rightarrow \ell^{+}\nu\ell^{-}\bar{\nu}b\bar{b}$), ℓ being an electron or a muon. The search has been optimized for the decay mode $H \rightarrow b\bar{b}$, however sensitivity to other decay modes has been preserved. Artificial neural networks are used to discriminate between signal and background events. Combining the results from the 7 TeV and 8 TeV samples, the observed (expected) limit on the cross section for Higgs boson production in association with top-quark pairs for a Higgs boson mass of 125 GeV is 5.8 (5.2) times the standard model expectation. This is the first such search at the LHC.

Acknowledgements

References

[1] ATLAS Collaboration, "Observation of a new particle in the search for the Standard Model Higgs boson with the ATLAS detector at the LHC", *Phys. Lett. B* **716** (2012) 1, `doi:10.1016/j.physletb.2012.08.020`, `arXiv:1207.7214`.

[2] CMS Collaboration, "Observation of a new boson at a mass of 125 GeV with the CMS experiment at the LHC", *Phys. Lett. B* **716** (2012) 30, `doi:10.1016/j.physletb.2012.08.021`, `arXiv:1207.7235`.

[3] H. M. Georgi et al., "Higgs Bosons from Two-Gluon Annihilation in Proton-Proton Collisions", *Phys. Rev. Lett.* **40** (1978) 692, `doi:10.1103/PhysRevLett.40.692`.

[4] S. Actis et al., "NNLO Computational Techniques: The Cases $H \rightarrow \gamma\gamma$ and $H \rightarrow gg$", *Nucl. Phys. B* **811** (2009) 182, `doi:10.1016/j.nuclphysb.2008.11.024`, `arXiv:0809.3667`.

[5] ALEPH, CDF, D0, DELPHI, L3, OPAL, and SLD Collaborations, the LEP Electroweak Working Group, the Tevatron Electroweak Working Group, and the SLD Electroweak and Heavy Flavour Groups, "Precision electroweak measurements and constraints on the Standard Model", (2010). `arXiv:1012.2367`.

[6] F. Maltoni, D. L. Rainwater, and S. Willenbrock, "Measuring the top quark Yukawa coupling at hadron colliders via $t\bar{t}H, H \rightarrow W^+W^-$", *Phys. Rev. D* **66** (2002) 034022, `doi:10.1103/PhysRevD.66.034022`, `arXiv:hep-ph/0202205`.

[7] A. Belyaev and L. Reina, "$pp \rightarrow t\bar{t}H, H \rightarrow \tau^+\tau^-$: Toward a model independent determination of the Higgs boson couplings at the LHC", *JHEP* **08** (2002) 041, `doi:10.1088/1126-6708/2002/08/041`, `arXiv:hep-ph/0205270`.

[8] C. Degrande et al., "Probing top-Higgs non-standard interactions at the LHC", *JHEP* **07** (2012) 036, `doi:10.1007/JHEP07(2012)036`, `arXiv:1205.1065`.

[9] A. Carmona, M. Chala, and J. Santiago, "New Higgs production mechanism in composite Higgs models", *JHEP* **07** (2012) 049, `doi:10.1007/JHEP07(2012)049`, `arXiv:1205.2378`.

[10] CDF Collaboration, "Search for the standard model Higgs boson produced in association with top quarks using the full CDF data set", *Phys. Rev. Lett.* **109** (2012) 181802, `doi:10.1103/PhysRevLett.109.181802`, `arXiv:1208.2662`.

[11] CMS Collaboration, "The CMS experiment at the CERN LHC", *JINST* **3** (2008) S08004, `doi:10.1088/1748-0221/3/08/S08004`.

[12] J. Alwall et al., "MadGraph 5: going beyond", *JHEP* **06** (2011) 128, `doi:10.1007/JHEP06(2011)128`, `arXiv:1106.0522`.

[13] T. Sjöstrand, S. Mrenna, and P. Z. Skands, "PYTHIA 6.4 physics and manual", *JHEP* **05** (2006) 026, `doi:10.1088/1126-6708/2006/05/026`, `arXiv:hep-ph/0603175`.

[14] S. Alioli et al., "A general framework for implementing NLO calculations in shower Monte Carlo programs: the POWHEG BOX", *JHEP* **06** (2010) 043, `doi:10.1007/JHEP06(2010)043`, `arXiv:1002.2581`.

[15] J. Pumplin et al., "New generation of parton distributions with uncertainties from global QCD analysis", *JHEP* **07** (2002) 012, `doi:10.1088/1126-6708/2002/07/012`, `arXiv:hep-ph/0201195`.

[16] N. Davidson et al., "Universal interface of TAUOLA: Technical and physics documentation", *Comput. Phys. Commun.* **183** (2012) 821, `doi:10.1016/j.cpc.2011.12.009`, `arXiv:1002.0543`.

[17] R. Raitio and W. W. Wada, "Higgs-boson production at large transverse momentum in quantum chromodynamics", *Phys. Rev. D* **19** (1979) 941, `doi:10.1103/PhysRevD.19.941`.

[18] J. N. Ng and P. Zakarauskas, "QCD-parton calculation of conjoined production of Higgs bosons and heavy flavors in p anti-p collisions", *Phys. Rev. D* **29** (1984) 876, doi:10.1103/PhysRevD.29.876.

[19] Z. Kunszt, "Associated production of heavy Higgs boson with top quarks", *Nucl. Phys. B* **247** (1984) 339, doi:10.1016/0550-3213(84)90553-4.

[20] W. Beenakker et al., "Higgs radiation off top quarks at the Tevatron and the LHC", *Phys. Rev. Lett.* **87** (2001) 201805, doi:10.1103/PhysRevLett.87.201805, arXiv:hep-ph/0107081.

[21] W. Beenakker et al., "NLO QCD corrections to t̄tH production in hadron collisions", *Nucl. Phys. B* **653** (2003) 151, doi:10.1016/S0550-3213(03)00044-0, arXiv:hep-ph/0211352.

[22] S. Dawson et al., "Associated top quark Higgs boson production at the LHC", *Phys. Rev. D* **67** (2003) 071503, doi:10.1103/PhysRevD.67.071503, arXiv:hep-ph/0211438.

[23] S. Dawson et al., "Associated Higgs production with top quarks at the large hadron collider: NLO QCD corrections", *Phys. Rev. D* **68** (2003) 034022, doi:10.1103/PhysRevD.68.034022, arXiv:hep-ph/0305087.

[24] LHC Higgs Cross Section Working Group, "Handbook of LHC Higgs Cross Sections: 1. Inclusive Observables", (2011). arXiv:1101.0593.

[25] A. Djouadi, J. Kalinowski, and M. Spira, "HDECAY: A program for Higgs boson decays in the standard model and its supersymmetric extension", *Comput. Phys. Commun.* **108** (1998) 56, doi:10.1016/S0010-4655(97)00123-9, arXiv:hep-ph/9704448.

[26] A. Djouadi, M. M. Muhlleitner, and M. Spira, "Decays of supersymmetric particles: The Program SUSY-HIT (SUspect-SdecaY-Hdecay-InTerface)", *Acta Phys. Polon. B* **38** (2007) 635, arXiv:hep-ph/0609292.

[27] A. Bredenstein et al., "Precise predictions for the Higgs-boson decay H → WW/ZZ → 4 leptons", *Phys. Rev. D* **74** (2006) 013004, doi:10.1103/PhysRevD.74.013004, arXiv:hep-ph/0604011.

[28] A. Bredenstein et al., "Radiative corrections to the semileptonic and hadronic Higgs-boson decays H → WW/ZZ → 4 fermions", *JHEP* **02** (2007) 080, doi:10.1088/1126-6708/2007/02/080, arXiv:hep-ph/0611234.

[29] M. Cacciari et al., "Updated predictions for the total production cross sections of top and of heavier quark pairs at the Tevatron and at the LHC", *JHEP* **09** (2008) 127, doi:10.1088/1126-6708/2008/09/127, arXiv:0804.2800.

[30] J. M. Campbell, R. K. Ellis, and C. Williams, "Vector boson pair production at the LHC", *JHEP* **07** (2011) 018, doi:10.1007/JHEP07(2011)018, arXiv:1105.0020.

[31] J. M. Campbell, R. K. Ellis, and C. Williams, "Gluon-gluon contributions to W+ W-production and Higgs interference effects", *JHEP* **10** (2011) 005, doi:10.1007/JHEP10(2011)005, arXiv:1107.5569.

[32] N. Kidonakis, "Differential and total cross sections for top pair and single top production", (2012). arXiv:1205.3453.

[33] N. Kidonakis, "Next-to-next-to-leading-order collinear and soft gluon corrections for t-channel single top quark production", *Phys. Rev. D* **83** (2011) 091503, `doi:10.1103/PhysRevD.83.091503`, `arXiv:1103.2792`.

[34] N. Kidonakis, "NNLL resummation for s-channel single top quark production", *Phys. Rev. D* **81** (2010) 054028, `doi:10.1103/PhysRevD.81.054028`, `arXiv:1001.5034`.

[35] N. Kidonakis, "Two-loop soft anomalous dimensions for single top quark associated production with a W^- or H^-", *Phys. Rev. D* **82** (2010) 054018, `doi:10.1103/PhysRevD.82.054018`, `arXiv:1005.4451`.

[36] R. Gavin et al., "FEWZ 2.0: A code for hadronic Z production at next-to-next-to-leading order", *Comput. Phys. Commun.* **182** (2011) 2388, `doi:10.1016/j.cpc.2011.06.008`, `arXiv:1011.3540`.

[37] R. Gavin et al., "W Physics at the LHC with FEWZ 2.1", (2012). `arXiv:1201.5896`.

[38] J. M. Campbell and R. K. Ellis, "$t\bar{t}W^{+-}$ production and decay at NLO", *JHEP* **07** (2012) 052, `doi:10.1007/JHEP07(2012)052`, `arXiv:1204.5678`.

[39] M. V. Garzelli et al., "$t\bar{t}W^{+-}$ and $t\bar{t}Z$ hadroproduction at NLO accuracy in QCD with parton shower and hadronization effects", *JHEP* **11** (2012) 056, `doi:10.1007/JHEP11(2012)056`, `arXiv:1208.2665`.

[40] GEANT4 Collaboration, "GEANT4—a simulation toolkit", *Nucl. Instrum. Meth. A* **506** (2003) 250, `doi:10.1016/S0168-9002(03)01368-8`.

[41] CMS Collaboration, "Determination of jet energy calibration and transverse momentum resolution in CMS", *JINST* **6** (2011) P11002, `doi:10.1088/1748-0221/6/11/P11002`, `arXiv:1107.4277`.

[42] CMS Collaboration, "Identification of b-quark jets with the CMS experiment", *JINST* **8** (2012) P04013, `doi:10.1088/1748-0221/8/04/P04013`, `arXiv:1211.4462`.

[43] CMS Collaboration, "Particle-Flow Event Reconstruction in CMS and Performance for Jets, Taus, and MET", CMS Physics Analysis Summary CMS-PAS-PFT-09-001, (2009).

[44] CMS Collaboration, "Performance of CMS muon reconstruction in pp collision events at $\sqrt{s} = 7$ TeV", *JINST* **7** (2012) P10002, `doi:10.1088/1748-0221/7/10/P10002`, `arXiv:1206.4071`.

[45] CMS Collaboration, "Electron reconstruction and identification at $\sqrt{s} = 7$ TeV", CMS Physics Analysis Summary CMS-PAS-EGM-10-004, (2010).

[46] M. Cacciari and G. P. Salam, "Dispelling the N^3 myth for the k_t jet-finder", *Phys. Lett. B* **641** (2006) 57, `doi:10.1016/j.physletb.2006.08.037`, `arXiv:hep-ph/0512210`.

[47] M. Cacciari, G. P. Salam, and G. Soyez, "The anti-k_t jet clustering algorithm", *JHEP* **04** (2008) 063, `doi:10.1088/1126-6708/2008/04/063`, `arXiv:0802.1189`.

[48] M. Cacciari, G. P. Salam, and G. Soyez, "The catchment area of jets", *JHEP* **04** (2008) 005, `doi:10.1088/1126-6708/2008/04/005`, `arXiv:0802.1188`.

[49] M. Cacciari and G. P. Salam, "Pileup subtraction using jet areas", *Phys. Lett. B* **659** (2008) 119, `doi:10.1016/j.physletb.2007.09.077`, `arXiv:0707.1378`.

[50] B. Ripley, "Pattern Recognition and Neural Networks". Cambridge University Press, 1996.

[51] H. Voss et al., "TMVA: Toolkit for Multivariate Data Analysis with ROOT", in *XIth International Workshop on Advanced Computing and Analysis Techniques in Physics Research (ACAT)*, p. 040. 2007. `arXiv:physics/0703039`.

[52] J. D. Bjorken and S. J. Brodsky, "Statistical Model for Electron-Positron Annihilation into Hadrons", *Phys. Rev. D* **1** (1970) 1416, `doi:10.1103/PhysRevD.1.1416`.

[53] G. C. Fox and S. Wolfram, "Event Shapes in e^+e^- Annihilation", *Nucl. Phys. B* **149** (1979) 413, `doi:10.1016/0550-3213(79)90003-8`.

[54] R. Brun and F. Rademakers, "ROOT: An object oriented data analysis framework", *Nucl. Instrum. Meth. A* **389** (1997) 81, `doi:10.1016/S0168-9002(97)00048-X`.

[55] CMS Collaboration, "Absolute Calibration of the Luminosity Measurement at CMS: Winter 2012 Update", CMS Physics Analysis Summary CMS-PAS-SMP-12-008, (2012).

[56] CMS Collaboration, "CMS Luminosity Based on Pixel Cluster Counting - Summer 2012 Update", CMS Physics Analysis Summary CMS-PAS-LUM-12-001, (2012).

[57] R. Barlow and C. Beeston, "Fitting using finite Monte Carlo samples", *Comput. Phys. Commun.* **77** (1993) 219, `doi:10.1016/0010-4655(93)90005-W`.

[58] J. S. Conway, "Incorporating Nuisance Parameters in Likelihoods for Multisource Spectra", (2011). `arXiv:1103.0354`.

[59] A. Bredenstein et al., "NLO QCD corrections to $t\bar{t}b\bar{b}$ production at the LHC: 2. Full hadronic results", *JHEP* **03** (2010) 021, `doi:10.1007/JHEP03(2010)021`, `arXiv:1001.4006`.

[60] CMS Collaboration, "Combined results of searches for the standard model Higgs boson in pp collisions at $\sqrt{s} = 7$ TeV", *Phys. Lett. B* **710** (2012) 26, `doi:10.1016/j.physletb.2012.02.064`, `arXiv:1202.1488`.

[61] ATLAS and CMS Collaborations, LHC Higgs Combination Group, "Procedure for the LHC Higgs boson search combination in Summer 2011", Technical Report CMS-NOTE-2011-005/ATL-PHYS-PUB-2011-11, CERN, Geneva, (Aug, 2011).

[62] T. Junk, "Confidence level computation for combining searches with small statistics", *Nucl. Instrum. Meth. A* **434** (1999) 435, `doi:10.1016/S0168-9002(99)00498-2`, `arXiv:hep-ex/9902006`.

[63] A. L. Read, "Presentation of search results: The CL_s technique", *J. Phys. G* **28** (2002) 2693, `doi:10.1088/0954-3899/28/10/313`.

A   The CMS Collaboration

Yerevan Physics Institute, Yerevan, Armenia
S. Chatrchyan, V. Khachatryan, A.M. Sirunyan, A. Tumasyan

Institut für Hochenergiephysik der OeAW, Wien, Austria
W. Adam, T. Bergauer, M. Dragicevic, J. Erö, C. Fabjan[1], M. Friedl, R. Frühwirth[1], V.M. Ghete, N. Hörmann, J. Hrubec, M. Jeitler[1], W. Kiesenhofer, V. Knünz, M. Krammer[1], I. Krätschmer, D. Liko, I. Mikulec, D. Rabady[2], B. Rahbaran, C. Rohringer, H. Rohringer, R. Schöfbeck, J. Strauss, A. Taurok, W. Treberer-treberspurg, W. Waltenberger, C.-E. Wulz[1]

National Centre for Particle and High Energy Physics, Minsk, Belarus
V. Mossolov, N. Shumeiko, J. Suarez Gonzalez

Universiteit Antwerpen, Antwerpen, Belgium
S. Alderweireldt, M. Bansal, S. Bansal, T. Cornelis, E.A. De Wolf, X. Janssen, A. Knutsson, S. Luyckx, L. Mucibello, S. Ochesanu, B. Roland, R. Rougny, H. Van Haevermaet, P. Van Mechelen, N. Van Remortel, A. Van Spilbeeck

Vrije Universiteit Brussel, Brussel, Belgium
F. Blekman, S. Blyweert, J. D'Hondt, R. Gonzalez Suarez, A. Kalogeropoulos, J. Keaveney, M. Maes, A. Olbrechts, S. Tavernier, W. Van Doninck, P. Van Mulders, G.P. Van Onsem, I. Villella

Université Libre de Bruxelles, Bruxelles, Belgium
B. Clerbaux, G. De Lentdecker, V. Dero, A.P.R. Gay, T. Hreus, A. Léonard, P.E. Marage, A. Mohammadi, T. Reis, L. Thomas, C. Vander Velde, P. Vanlaer, J. Wang

Ghent University, Ghent, Belgium
V. Adler, K. Beernaert, L. Benucci, A. Cimmino, S. Costantini, G. Garcia, M. Grunewald, B. Klein, J. Lellouch, A. Marinov, J. Mccartin, A.A. Ocampo Rios, D. Ryckbosch, M. Sigamani, N. Strobbe, F. Thyssen, M. Tytgat, S. Walsh, E. Yazgan, N. Zaganidis

Université Catholique de Louvain, Louvain-la-Neuve, Belgium
S. Basegmez, G. Bruno, R. Castello, L. Ceard, C. Delaere, T. du Pree, D. Favart, L. Forthomme, A. Giammanco[3], J. Hollar, V. Lemaitre, J. Liao, O. Militaru, C. Nuttens, D. Pagano, A. Pin, K. Piotrzkowski, A. Popov[4], M. Selvaggi, J.M. Vizan Garcia

Université de Mons, Mons, Belgium
N. Beliy, T. Caebergs, E. Daubie, G.H. Hammad

Centro Brasileiro de Pesquisas Fisicas, Rio de Janeiro, Brazil
G.A. Alves, M. Correa Martins Junior, T. Martins, M.E. Pol, M.H.G. Souza

Universidade do Estado do Rio de Janeiro, Rio de Janeiro, Brazil
W.L. Aldá Júnior, W. Carvalho, J. Chinellato[5], A. Custódio, E.M. Da Costa, D. De Jesus Damiao, C. De Oliveira Martins, S. Fonseca De Souza, H. Malbouisson, M. Malek, D. Matos Figueiredo, L. Mundim, H. Nogima, W.L. Prado Da Silva, A. Santoro, L. Soares Jorge, A. Sznajder, E.J. Tonelli Manganote[5], A. Vilela Pereira

Universidade Estadual Paulista [a], Universidade Federal do ABC [b], São Paulo, Brazil
T.S. Anjos[b], C.A. Bernardes[b], F.A. Dias[a,6], T.R. Fernandez Perez Tomei[a], E.M. Gregores[b], C. Lagana[a], F. Marinho[a], P.G. Mercadante[b], S.F. Novaes[a], Sandra S. Padula[a]

Institute for Nuclear Research and Nuclear Energy, Sofia, Bulgaria
V. Genchev[2], P. Iaydjiev[2], S. Piperov, M. Rodozov, S. Stoykova, G. Sultanov, V. Tcholakov, R. Trayanov, M. Vutova

University of Sofia, Sofia, Bulgaria
A. Dimitrov, R. Hadjiiska, V. Kozhuharov, L. Litov, B. Pavlov, P. Petkov

Institute of High Energy Physics, Beijing, China
J.G. Bian, G.M. Chen, H.S. Chen, C.H. Jiang, D. Liang, S. Liang, X. Meng, J. Tao, J. Wang, X. Wang, Z. Wang, H. Xiao, M. Xu

State Key Laboratory of Nuclear Physics and Technology, Peking University, Beijing, China
C. Asawatangtrakuldee, Y. Ban, Y. Guo, Q. Li, W. Li, S. Liu, Y. Mao, S.J. Qian, D. Wang, L. Zhang, W. Zou

Universidad de Los Andes, Bogota, Colombia
C. Avila, C.A. Carrillo Montoya, J.P. Gomez, B. Gomez Moreno, J.C. Sanabria

Technical University of Split, Split, Croatia
N. Godinovic, D. Lelas, R. Plestina[7], D. Polic, I. Puljak

University of Split, Split, Croatia
Z. Antunovic, M. Kovac

Institute Rudjer Boskovic, Zagreb, Croatia
V. Brigljevic, S. Duric, K. Kadija, J. Luetic, D. Mekterovic, S. Morovic, L. Tikvica

University of Cyprus, Nicosia, Cyprus
A. Attikis, G. Mavromanolakis, J. Mousa, C. Nicolaou, F. Ptochos, P.A. Razis

Charles University, Prague, Czech Republic
M. Finger, M. Finger Jr.

Academy of Scientific Research and Technology of the Arab Republic of Egypt, Egyptian Network of High Energy Physics, Cairo, Egypt
Y. Assran[8], A. Ellithi Kamel[9], A.M. Kuotb Awad[10], M.A. Mahmoud[10], A. Radi[11,12]

National Institute of Chemical Physics and Biophysics, Tallinn, Estonia
M. Kadastik, M. Müntel, M. Murumaa, M. Raidal, L. Rebane, A. Tiko

Department of Physics, University of Helsinki, Helsinki, Finland
P. Eerola, G. Fedi, M. Voutilainen

Helsinki Institute of Physics, Helsinki, Finland
J. Härkönen, V. Karimäki, R. Kinnunen, M.J. Kortelainen, T. Lampén, K. Lassila-Perini, S. Lehti, T. Lindén, P. Luukka, T. Mäenpää, T. Peltola, E. Tuominen, J. Tuominiemi, E. Tuovinen, L. Wendland

Lappeenranta University of Technology, Lappeenranta, Finland
A. Korpela, T. Tuuva

DSM/IRFU, CEA/Saclay, Gif-sur-Yvette, France
M. Besancon, S. Choudhury, F. Couderc, M. Dejardin, D. Denegri, B. Fabbro, J.L. Faure, F. Ferri, S. Ganjour, A. Givernaud, P. Gras, G. Hamel de Monchenault, P. Jarry, E. Locci, J. Malcles, L. Millischer, A. Nayak, J. Rander, A. Rosowsky, M. Titov

Laboratoire Leprince-Ringuet, Ecole Polytechnique, IN2P3-CNRS, Palaiseau, France
S. Baffioni, F. Beaudette, L. Benhabib, L. Bianchini, M. Bluj[13], P. Busson, C. Charlot, N. Daci, T. Dahms, M. Dalchenko, L. Dobrzynski, A. Florent, R. Granier de Cassagnac, M. Haguenauer, P. Miné, C. Mironov, I.N. Naranjo, M. Nguyen, C. Ochando, P. Paganini, D. Sabes, R. Salerno, Y. Sirois, C. Veelken, A. Zabi

Institut Pluridisciplinaire Hubert Curien, Université de Strasbourg, Université de Haute Alsace Mulhouse, CNRS/IN2P3, Strasbourg, France

J.-L. Agram[14], J. Andrea, D. Bloch, D. Bodin, J.-M. Brom, E.C. Chabert, C. Collard, E. Conte[14], F. Drouhin[14], J.-C. Fontaine[14], D. Gelé, U. Goerlach, C. Goetzmann, P. Juillot, A.-C. Le Bihan, P. Van Hove

Université de Lyon, Université Claude Bernard Lyon 1, CNRS-IN2P3, Institut de Physique Nucléaire de Lyon, Villeurbanne, France

S. Beauceron, N. Beaupere, O. Bondu, G. Boudoul, S. Brochet, J. Chasserat, R. Chierici[2], D. Contardo, P. Depasse, H. El Mamouni, J. Fay, S. Gascon, M. Gouzevitch, B. Ille, T. Kurca, M. Lethuillier, L. Mirabito, S. Perries, L. Sgandurra, V. Sordini, Y. Tschudi, M. Vander Donckt, P. Verdier, S. Viret

Institute of High Energy Physics and Informatization, Tbilisi State University, Tbilisi, Georgia

Z. Tsamalaidze[15]

RWTH Aachen University, I. Physikalisches Institut, Aachen, Germany

C. Autermann, S. Beranek, B. Calpas, M. Edelhoff, L. Feld, N. Heracleous, O. Hindrichs, R. Jussen, K. Klein, J. Merz, A. Ostapchuk, A. Perieanu, F. Raupach, J. Sammet, S. Schael, D. Sprenger, H. Weber, B. Wittmer, V. Zhukov[4]

RWTH Aachen University, III. Physikalisches Institut A, Aachen, Germany

M. Ata, J. Caudron, E. Dietz-Laursonn, D. Duchardt, M. Erdmann, R. Fischer, A. Güth, T. Hebbeker, C. Heidemann, K. Hoepfner, D. Klingebiel, P. Kreuzer, M. Merschmeyer, A. Meyer, M. Olschewski, K. Padeken, P. Papacz, H. Pieta, H. Reithler, S.A. Schmitz, L. Sonnenschein, J. Steggemann, D. Teyssier, S. Thüer, M. Weber

RWTH Aachen University, III. Physikalisches Institut B, Aachen, Germany

M. Bontenackels, V. Cherepanov, Y. Erdogan, G. Flügge, H. Geenen, M. Geisler, W. Haj Ahmad, F. Hoehle, B. Kargoll, T. Kress, Y. Kuessel, J. Lingemann[2], A. Nowack, I.M. Nugent, L. Perchalla, O. Pooth, A. Stahl

Deutsches Elektronen-Synchrotron, Hamburg, Germany

M. Aldaya Martin, I. Asin, N. Bartosik, J. Behr, W. Behrenhoff, U. Behrens, M. Bergholz[16], A. Bethani, K. Borras, A. Burgmeier, A. Cakir, L. Calligaris, A. Campbell, F. Costanza, D. Dammann, C. Diez Pardos, T. Dorland, G. Eckerlin, D. Eckstein, G. Flucke, A. Geiser, I. Glushkov, P. Gunnellini, S. Habib, J. Hauk, G. Hellwig, H. Jung, M. Kasemann, P. Katsas, C. Kleinwort, H. Kluge, M. Krämer, D. Krücker, E. Kuznetsova, W. Lange, J. Leonard, W. Lohmann[16], B. Lutz, R. Mankel, I. Marfin, M. Marienfeld, I.-A. Melzer-Pellmann, A.B. Meyer, J. Mnich, A. Mussgiller, S. Naumann-Emme, O. Novgorodova, F. Nowak, J. Olzem, H. Perrey, A. Petrukhin, D. Pitzl, A. Raspereza, P.M. Ribeiro Cipriano, C. Riedl, E. Ron, M. Rosin, J. Salfeld-Nebgen, R. Schmidt[16], T. Schoerner-Sadenius, N. Sen, M. Stein, R. Walsh, C. Wissing

University of Hamburg, Hamburg, Germany

V. Blobel, H. Enderle, J. Erfle, U. Gebbert, M. Görner, M. Gosselink, J. Haller, R.S. Höing, K. Kaschube, G. Kaussen, H. Kirschenmann, R. Klanner, J. Lange, T. Peiffer, N. Pietsch, D. Rathjens, C. Sander, H. Schettler, P. Schleper, E. Schlieckau, A. Schmidt, T. Schum, M. Seidel, J. Sibille[17], V. Sola, H. Stadie, G. Steinbrück, J. Thomsen, L. Vanelderen

Institut für Experimentelle Kernphysik, Karlsruhe, Germany

C. Barth, C. Baus, J. Berger, C. Böser, T. Chwalek, W. De Boer, A. Descroix, A. Dierlamm,

M. Feindt, M. Guthoff[2], C. Hackstein, F. Hartmann[2], T. Hauth[2], M. Heinrich, H. Held, K.H. Hoffmann, U. Husemann, I. Katkov[4], J.R. Komaragiri, A. Kornmayer[2], P. Lobelle Pardo, D. Martschei, S. Mueller, Th. Müller, M. Niegel, A. Nürnberg, O. Oberst, J. Ott, G. Quast, K. Rabbertz, F. Ratnikov, N. Ratnikova, S. Röcker, F.-P. Schilling, G. Schott, H.J. Simonis, F.M. Stober, D. Troendle, R. Ulrich, J. Wagner-Kuhr, S. Wayand, T. Weiler, M. Zeise

Institute of Nuclear Physics "Demokritos", Aghia Paraskevi, Greece
G. Anagnostou, G. Daskalakis, T. Geralis, S. Kesisoglou, A. Kyriakis, D. Loukas, A. Markou, C. Markou, E. Ntomari

University of Athens, Athens, Greece
L. Gouskos, T.J. Mertzimekis, A. Panagiotou, N. Saoulidou, E. Stiliaris

University of Ioánnina, Ioánnina, Greece
X. Aslanoglou, I. Evangelou, G. Flouris, C. Foudas, P. Kokkas, N. Manthos, I. Papadopoulos, E. Paradas

KFKI Research Institute for Particle and Nuclear Physics, Budapest, Hungary
G. Bencze, C. Hajdu, P. Hidas, D. Horvath[18], B. Radics, F. Sikler, V. Veszpremi, G. Vesztergombi[19], A.J. Zsigmond

Institute of Nuclear Research ATOMKI, Debrecen, Hungary
N. Beni, S. Czellar, J. Molnar, J. Palinkas, Z. Szillasi

University of Debrecen, Debrecen, Hungary
J. Karancsi, P. Raics, Z.L. Trocsanyi, B. Ujvari

Panjab University, Chandigarh, India
S.B. Beri, V. Bhatnagar, N. Dhingra, R. Gupta, M. Kaur, M.Z. Mehta, M. Mittal, N. Nishu, L.K. Saini, A. Sharma, J.B. Singh

University of Delhi, Delhi, India
Ashok Kumar, Arun Kumar, S. Ahuja, A. Bhardwaj, B.C. Choudhary, S. Malhotra, M. Naimuddin, K. Ranjan, P. Saxena, V. Sharma, R.K. Shivpuri

Saha Institute of Nuclear Physics, Kolkata, India
S. Banerjee, S. Bhattacharya, K. Chatterjee, S. Dutta, B. Gomber, Sa. Jain, Sh. Jain, R. Khurana, A. Modak, S. Mukherjee, D. Roy, S. Sarkar, M. Sharan

Bhabha Atomic Research Centre, Mumbai, India
A. Abdulsalam, D. Dutta, S. Kailas, V. Kumar, A.K. Mohanty[2], L.M. Pant, P. Shukla, A. Topkar

Tata Institute of Fundamental Research - EHEP, Mumbai, India
T. Aziz, R.M. Chatterjee, S. Ganguly, M. Guchait[20], A. Gurtu[21], M. Maity[22], G. Majumder, K. Mazumdar, G.B. Mohanty, B. Parida, K. Sudhakar, N. Wickramage

Tata Institute of Fundamental Research - HECR, Mumbai, India
S. Banerjee, S. Dugad

Institute for Research in Fundamental Sciences (IPM), Tehran, Iran
H. Arfaei[23], H. Bakhshiansohi, S.M. Etesami[24], A. Fahim[23], H. Hesari, A. Jafari, M. Khakzad, M. Mohammadi Najafabadi, S. Paktinat Mehdiabadi, B. Safarzadeh[25], M. Zeinali

INFN Sezione di Bari [a], Università di Bari [b], Politecnico di Bari [c], Bari, Italy
M. Abbrescia[a,b], L. Barbone[a,b], C. Calabria[a,b,2], S.S. Chhibra[a,b], A. Colaleo[a], D. Creanza[a,c], N. De Filippis[a,c,2], M. De Palma[a,b], L. Fiore[a], G. Iaselli[a,c], G. Maggi[a,c], M. Maggi[a], B. Marangelli[a,b],

S. My[a,c], S. Nuzzo[a,b], N. Pacifico[a], A. Pompili[a,b], G. Pugliese[a,c], G. Selvaggi[a,b], L. Silvestris[a], G. Singh[a,b], R. Venditti[a,b], P. Verwilligen[a], G. Zito[a]

INFN Sezione di Bologna [a], Università di Bologna [b], Bologna, Italy
G. Abbiendi[a], A.C. Benvenuti[a], D. Bonacorsi[a,b], S. Braibant-Giacomelli[a,b], L. Brigliadori[a,b], R. Campanini[a,b], P. Capiluppi[a,b], A. Castro[a,b], F.R. Cavallo[a], M. Cuffiani[a,b], G.M. Dallavalle[a], F. Fabbri[a], A. Fanfani[a,b], D. Fasanella[a,b], P. Giacomelli[a], C. Grandi[a], L. Guiducci[a,b], S. Marcellini[a], G. Masetti[a], M. Meneghelli[a,b,2], A. Montanari[a], F.L. Navarria[a,b], F. Odorici[a], A. Perrotta[a], F. Primavera[a,b], A.M. Rossi[a,b], T. Rovelli[a,b], G.P. Siroli[a,b], N. Tosi[a,b], R. Travaglini[a,b]

INFN Sezione di Catania [a], Università di Catania [b], Catania, Italy
S. Albergo[a,b], M. Chiorboli[a,b], S. Costa[a,b], R. Potenza[a,b], A. Tricomi[a,b], C. Tuve[a,b]

INFN Sezione di Firenze [a], Università di Firenze [b], Firenze, Italy
G. Barbagli[a], V. Ciulli[a,b], C. Civinini[a], R. D'Alessandro[a,b], E. Focardi[a,b], S. Frosali[a,b], E. Gallo[a], S. Gonzi[a,b], P. Lenzi[a,b], M. Meschini[a], S. Paoletti[a], G. Sguazzoni[a], A. Tropiano[a,b]

INFN Laboratori Nazionali di Frascati, Frascati, Italy
L. Benussi, S. Bianco, S. Colafranceschi[26], F. Fabbri, D. Piccolo

INFN Sezione di Genova [a], Università di Genova [b], Genova, Italy
P. Fabbricatore[a], R. Musenich[a], S. Tosi[a,b]

INFN Sezione di Milano-Bicocca [a], Università di Milano-Bicocca [b], Milano, Italy
A. Benaglia[a], F. De Guio[a,b], L. Di Matteo[a,b,2], S. Fiorendi[a,b], S. Gennai[a,2], A. Ghezzi[a,b], M.T. Lucchini[2], S. Malvezzi[a], R.A. Manzoni[a,b], A. Martelli[a,b], A. Massironi[a,b], D. Menasce[a], L. Moroni[a], M. Paganoni[a,b], D. Pedrini[a], S. Ragazzi[a,b], N. Redaelli[a], T. Tabarelli de Fatis[a,b]

INFN Sezione di Napoli [a], Università di Napoli 'Federico II' [b], Università della Basilicata (Potenza) [c], Università G. Marconi (Roma) [d], Napoli, Italy
S. Buontempo[a], N. Cavallo[a,c], A. De Cosa[a,b,2], O. Dogangun[a,b], F. Fabozzi[a,c], A.O.M. Iorio[a,b], L. Lista[a], S. Meola[a,d,2], M. Merola[a], P. Paolucci[a,2]

INFN Sezione di Padova [a], Università di Padova [b], Università di Trento (Trento) [c], Padova, Italy
P. Azzi[a], N. Bacchetta[a,2], M. Biasotto[a,27], D. Bisello[a,b], A. Branca[a,b], R. Carlin[a,b], P. Checchia[a], T. Dorigo[a], M. Galanti[a,b], F. Gasparini[a,b], U. Gasparini[a,b], P. Giubilato[a,b], A. Gozzelino[a], K. Kanishchev[a,c], S. Lacaprara[a], I. Lazzizzera[a,c], M. Margoni[a,b], A.T. Meneguzzo[a,b], M. Passaseo[a], J. Pazzini[a,b], N. Pozzobon[a,b], P. Ronchese[a,b], F. Simonetto[a,b], E. Torassa[a], M. Tosi[a,b], S. Vanini[a,b], S. Ventura[a], P. Zotto[a,b], A. Zucchetta[a,b], G. Zumerle[a,b]

INFN Sezione di Pavia [a], Università di Pavia [b], Pavia, Italy
M. Gabusi[a,b], S.P. Ratti[a,b], C. Riccardi[a,b], P. Vitulo[a,b]

INFN Sezione di Perugia [a], Università di Perugia [b], Perugia, Italy
M. Biasini[a,b], G.M. Bilei[a], L. Fanò[a,b], P. Lariccia[a,b], G. Mantovani[a,b], M. Menichelli[a], A. Nappi[a,b,†], F. Romeo[a,b], A. Saha[a], A. Santocchia[a,b], A. Spiezia[a,b], S. Taroni[a,b]

INFN Sezione di Pisa [a], Università di Pisa [b], Scuola Normale Superiore di Pisa [c], Pisa, Italy
P. Azzurri[a,c], G. Bagliesi[a], T. Boccali[a], G. Broccolo[a,c], R. Castaldi[a], R.T. D'Agnolo[a,c,2], R. Dell'Orso[a], F. Fiori[a,b,2], L. Foà[a,c], A. Giassi[a], A. Kraan[a], F. Ligabue[a,c], T. Lomtadze[a], L. Martini[a,28], A. Messineo[a,b], F. Palla[a], A. Rizzi[a,b], A.T. Serban[a], P. Spagnolo[a], P. Squillacioti[a], R. Tenchini[a], G. Tonelli[a,b], A. Venturi[a], P.G. Verdini[a], C. Vernieri[a,c]

INFN Sezione di Roma [a], Università di Roma [b], Roma, Italy
L. Barone[a,b], F. Cavallari[a], D. Del Re[a,b], M. Diemoz[a], C. Fanelli[a,b], M. Grassi[a,b,2], E. Longo[a,b], F. Margaroli[a,b], P. Meridiani[a,2], F. Micheli[a,b], S. Nourbakhsh[a,b], G. Organtini[a,b], R. Paramatti[a], S. Rahatlou[a,b], L. Soffi[a,b]

INFN Sezione di Torino [a], Università di Torino [b], Università del Piemonte Orientale (Novara) [c], Torino, Italy
N. Amapane[a,b], R. Arcidiacono[a,c], S. Argiro[a,b], M. Arneodo[a,c], C. Biino[a], N. Cartiglia[a], S. Casasso[a,b], M. Costa[a,b], N. Demaria[a], C. Mariotti[a,2], S. Maselli[a], E. Migliore[a,b], V. Monaco[a,b], M. Musich[a,2], M.M. Obertino[a,c], G. Ortona[a,b], N. Pastrone[a], M. Pelliccioni[a], A. Potenza[a,b], A. Romero[a,b], R. Sacchi[a,b], A. Solano[a,b], A. Staiano[a], U. Tamponi[a]

INFN Sezione di Trieste [a], Università di Trieste [b], Trieste, Italy
S. Belforte[a], V. Candelise[a,b], M. Casarsa[a], F. Cossutti[a,2], G. Della Ricca[a,b], B. Gobbo[a], M. Marone[a,b,2], D. Montanino[a,b], A. Penzo[a], A. Schizzi[a,b], A. Zanetti[a]

Kangwon National University, Chunchon, Korea
T.Y. Kim, S.K. Nam

Kyungpook National University, Daegu, Korea
S. Chang, D.H. Kim, G.N. Kim, J.E. Kim, D.J. Kong, Y.D. Oh, H. Park, D.C. Son

Chonnam National University, Institute for Universe and Elementary Particles, Kwangju, Korea
J.Y. Kim, Zero J. Kim, S. Song

Korea University, Seoul, Korea
S. Choi, D. Gyun, B. Hong, M. Jo, H. Kim, T.J. Kim, K.S. Lee, D.H. Moon, S.K. Park, Y. Roh

University of Seoul, Seoul, Korea
M. Choi, J.H. Kim, C. Park, I.C. Park, S. Park, G. Ryu

Sungkyunkwan University, Suwon, Korea
Y. Choi, Y.K. Choi, J. Goh, M.S. Kim, E. Kwon, B. Lee, J. Lee, S. Lee, H. Seo, I. Yu

Vilnius University, Vilnius, Lithuania
I. Grigelionis, A. Juodagalvis

Centro de Investigacion y de Estudios Avanzados del IPN, Mexico City, Mexico
H. Castilla-Valdez, E. De La Cruz-Burelo, I. Heredia-de La Cruz, R. Lopez-Fernandez, J. Martínez-Ortega, A. Sanchez-Hernandez, L.M. Villasenor-Cendejas

Universidad Iberoamericana, Mexico City, Mexico
S. Carrillo Moreno, F. Vazquez Valencia

Benemerita Universidad Autonoma de Puebla, Puebla, Mexico
H.A. Salazar Ibarguen

Universidad Autónoma de San Luis Potosí, San Luis Potosí, Mexico
E. Casimiro Linares, A. Morelos Pineda, M.A. Reyes-Santos

University of Auckland, Auckland, New Zealand
D. Krofcheck

University of Canterbury, Christchurch, New Zealand
A.J. Bell, P.H. Butler, R. Doesburg, S. Reucroft, H. Silverwood

National Centre for Physics, Quaid-I-Azam University, Islamabad, Pakistan
M. Ahmad, M.I. Asghar, J. Butt, H.R. Hoorani, S. Khalid, W.A. Khan, T. Khurshid, S. Qazi, M.A. Shah, M. Shoaib

National Centre for Nuclear Research, Swierk, Poland
H. Bialkowska, B. Boimska, T. Frueboes, M. Górski, M. Kazana, K. Nawrocki, K. Romanowska-Rybinska, M. Szleper, G. Wrochna, P. Zalewski

Institute of Experimental Physics, Faculty of Physics, University of Warsaw, Warsaw, Poland
G. Brona, K. Bunkowski, M. Cwiok, W. Dominik, K. Doroba, A. Kalinowski, M. Konecki, J. Krolikowski, M. Misiura, W. Wolszczak

Laboratório de Instrumentação e Física Experimental de Partículas, Lisboa, Portugal
N. Almeida, P. Bargassa, A. David, P. Faccioli, P.G. Ferreira Parracho, M. Gallinaro, J. Seixas[2], J. Varela, P. Vischia

Joint Institute for Nuclear Research, Dubna, Russia
P. Bunin, I. Golutvin, I. Gorbunov, V. Karjavin, V. Konoplyanikov, G. Kozlov, A. Lanev, A. Malakhov, P. Moisenz, V. Palichik, V. Perelygin, M. Savina, S. Shmatov, S. Shulha, V. Smirnov, A. Volodko, A. Zarubin

Petersburg Nuclear Physics Institute, Gatchina (St. Petersburg), Russia
S. Evstyukhin, V. Golovtsov, Y. Ivanov, V. Kim, P. Levchenko, V. Murzin, V. Oreshkin, I. Smirnov, V. Sulimov, L. Uvarov, S. Vavilov, A. Vorobyev, An. Vorobyev

Institute for Nuclear Research, Moscow, Russia
Yu. Andreev, A. Dermenev, S. Gninenko, N. Golubev, M. Kirsanov, N. Krasnikov, V. Matveev, A. Pashenkov, D. Tlisov, A. Toropin

Institute for Theoretical and Experimental Physics, Moscow, Russia
V. Epshteyn, M. Erofeeva, V. Gavrilov, N. Lychkovskaya, V. Popov, G. Safronov, S. Semenov, A. Spiridonov, V. Stolin, E. Vlasov, A. Zhokin

P.N. Lebedev Physical Institute, Moscow, Russia
V. Andreev, M. Azarkin, I. Dremin, M. Kirakosyan, A. Leonidov, G. Mesyats, S.V. Rusakov, A. Vinogradov

Skobeltsyn Institute of Nuclear Physics, Lomonosov Moscow State University, Moscow, Russia
A. Belyaev, E. Boos, V. Bunichev, M. Dubinin[6], L. Dudko, A. Ershov, A. Gribushin, V. Klyukhin, O. Kodolova, I. Lokhtin, A. Markina, S. Obraztsov, S. Petrushanko, V. Savrin

State Research Center of Russian Federation, Institute for High Energy Physics, Protvino, Russia
I. Azhgirey, I. Bayshev, S. Bitioukov, V. Kachanov, A. Kalinin, D. Konstantinov, V. Krychkine, V. Petrov, R. Ryutin, A. Sobol, L. Tourtchanovitch, S. Troshin, N. Tyurin, A. Uzunian, A. Volkov

University of Belgrade, Faculty of Physics and Vinca Institute of Nuclear Sciences, Belgrade, Serbia
P. Adzic[29], M. Ekmedzic, D. Krpic[29], J. Milosevic

Centro de Investigaciones Energéticas Medioambientales y Tecnológicas (CIEMAT), Madrid, Spain
M. Aguilar-Benitez, J. Alcaraz Maestre, C. Battilana, E. Calvo, M. Cerrada, M. Chamizo Llatas[2], N. Colino, B. De La Cruz, A. Delgado Peris, D. Domínguez Vázquez, C. Fernandez Bedoya,

J.P. Fernández Ramos, A. Ferrando, J. Flix, M.C. Fouz, P. Garcia-Abia, O. Gonzalez Lopez, S. Goy Lopez, J.M. Hernandez, M.I. Josa, G. Merino, J. Puerta Pelayo, A. Quintario Olmeda, I. Redondo, L. Romero, J. Santaolalla, M.S. Soares, C. Willmott

Universidad Autónoma de Madrid, Madrid, Spain
C. Albajar, J.F. de Trocóniz

Universidad de Oviedo, Oviedo, Spain
H. Brun, J. Cuevas, J. Fernandez Menendez, S. Folgueras, I. Gonzalez Caballero, L. Lloret Iglesias, J. Piedra Gomez

Instituto de Física de Cantabria (IFCA), CSIC-Universidad de Cantabria, Santander, Spain
J.A. Brochero Cifuentes, I.J. Cabrillo, A. Calderon, S.H. Chuang, J. Duarte Campderros, M. Fernandez, G. Gomez, J. Gonzalez Sanchez, A. Graziano, C. Jorda, A. Lopez Virto, J. Marco, R. Marco, C. Martinez Rivero, F. Matorras, F.J. Munoz Sanchez, T. Rodrigo, A.Y. Rodríguez-Marrero, A. Ruiz-Jimeno, L. Scodellaro, I. Vila, R. Vilar Cortabitarte

CERN, European Organization for Nuclear Research, Geneva, Switzerland
D. Abbaneo, E. Auffray, G. Auzinger, M. Bachtis, P. Baillon, A.H. Ball, D. Barney, J. Bendavid, J.F. Benitez, C. Bernet[7], G. Bianchi, P. Bloch, A. Bocci, A. Bonato, C. Botta, H. Breuker, T. Camporesi, G. Cerminara, T. Christiansen, J.A. Coarasa Perez, D. d'Enterria, A. Dabrowski, A. De Roeck, S. De Visscher, S. Di Guida, M. Dobson, N. Dupont-Sagorin, A. Elliott-Peisert, J. Eugster, W. Funk, G. Georgiou, M. Giffels, D. Gigi, K. Gill, D. Giordano, M. Giunta, F. Glege, R. Gomez-Reino Garrido, P. Govoni, S. Gowdy, R. Guida, J. Hammer, M. Hansen, P. Harris, C. Hartl, J. Harvey, B. Hegner, A. Hinzmann, V. Innocente, P. Janot, K. Kaadze, E. Karavakis, K. Kousouris, K. Krajczar, P. Lecoq, Y.-J. Lee, C. Lourenço, M. Malberti, L. Malgeri, M. Mannelli, L. Masetti, F. Meijers, S. Mersi, E. Meschi, R. Moser, M. Mulders, P. Musella, E. Nesvold, L. Orsini, E. Palencia Cortezon, E. Perez, L. Perrozzi, A. Petrilli, A. Pfeiffer, M. Pierini, M. Pimiä, D. Piparo, G. Polese, L. Quertenmont, A. Racz, W. Reece, J. Rodrigues Antunes, G. Rolandi[30], C. Rovelli[31], M. Rovere, H. Sakulin, F. Santanastasio, C. Schäfer, C. Schwick, I. Segoni, S. Sekmen, A. Sharma, P. Siegrist, P. Silva, M. Simon, P. Sphicas[32], D. Spiga, M. Stoye, A. Tsirou, G.I. Veres[19], J.R. Vlimant, H.K. Wöhri, S.D. Worm[33], W.D. Zeuner

Paul Scherrer Institut, Villigen, Switzerland
W. Bertl, K. Deiters, W. Erdmann, K. Gabathuler, R. Horisberger, Q. Ingram, H.C. Kaestli, S. König, D. Kotlinski, U. Langenegger, F. Meier, D. Renker, T. Rohe

Institute for Particle Physics, ETH Zurich, Zurich, Switzerland
F. Bachmair, L. Bäni, P. Bortignon, M.A. Buchmann, B. Casal, N. Chanon, A. Deisher, G. Dissertori, M. Dittmar, M. Donegà, M. Dünser, P. Eller, C. Grab, D. Hits, P. Lecomte, W. Lustermann, A.C. Marini, P. Martinez Ruiz del Arbol, N. Mohr, F. Moortgat, C. Nägeli[34], P. Nef, F. Nessi-Tedaldi, F. Pandolfi, L. Pape, F. Pauss, M. Peruzzi, F.J. Ronga, M. Rossini, L. Sala, A.K. Sanchez, A. Starodumov[35], B. Stieger, M. Takahashi, L. Tauscher[†], A. Thea, K. Theofilatos, D. Treille, C. Urscheler, R. Wallny, H.A. Weber

Universität Zürich, Zurich, Switzerland
C. Amsler[36], V. Chiochia, C. Favaro, M. Ivova Rikova, B. Kilminster, B. Millan Mejias, P. Otiougova, P. Robmann, H. Snoek, S. Tupputi, M. Verzetti

National Central University, Chung-Li, Taiwan
M. Cardaci, K.H. Chen, C. Ferro, C.M. Kuo, S.W. Li, W. Lin, Y.J. Lu, R. Volpe, S.S. Yu

National Taiwan University (NTU), Taipei, Taiwan
P. Bartalini, P. Chang, Y.H. Chang, Y.W. Chang, Y. Chao, K.F. Chen, C. Dietz, U. Grundler, W.-

S. Hou, Y. Hsiung, K.Y. Kao, Y.J. Lei, R.-S. Lu, D. Majumder, E. Petrakou, X. Shi, J.G. Shiu, Y.M. Tzeng, M. Wang

Chulalongkorn University, Bangkok, Thailand
B. Asavapibhop, N. Suwonjandee

Cukurova University, Adana, Turkey
A. Adiguzel, M.N. Bakirci[37], S. Cerci[38], C. Dozen, I. Dumanoglu, E. Eskut, S. Girgis, G. Gokbulut, E. Gurpinar, I. Hos, E.E. Kangal, A. Kayis Topaksu, G. Onengut, K. Ozdemir, S. Ozturk[39], A. Polatoz, K. Sogut[40], D. Sunar Cerci[38], B. Tali[38], H. Topakli[37], M. Vergili

Middle East Technical University, Physics Department, Ankara, Turkey
I.V. Akin, T. Aliev, B. Bilin, S. Bilmis, M. Deniz, H. Gamsizkan, A.M. Guler, G. Karapinar[41], K. Ocalan, A. Ozpineci, M. Serin, R. Sever, U.E. Surat, M. Yalvac, M. Zeyrek

Bogazici University, Istanbul, Turkey
E. Gülmez, B. Isildak[42], M. Kaya[43], O. Kaya[43], S. Ozkorucuklu[44], N. Sonmez[45]

Istanbul Technical University, Istanbul, Turkey
H. Bahtiyar[46], E. Barlas, K. Cankocak, Y.O. Günaydin[47], F.I. Vardarlı, M. Yücel

National Scientific Center, Kharkov Institute of Physics and Technology, Kharkov, Ukraine
L. Levchuk, P. Sorokin

University of Bristol, Bristol, United Kingdom
J.J. Brooke, E. Clement, D. Cussans, H. Flacher, R. Frazier, J. Goldstein, M. Grimes, G.P. Heath, H.F. Heath, L. Kreczko, S. Metson, D.M. Newbold[33], K. Nirunpong, A. Poll, S. Senkin, V.J. Smith, T. Williams

Rutherford Appleton Laboratory, Didcot, United Kingdom
L. Basso[48], K.W. Bell, A. Belyaev[48], C. Brew, R.M. Brown, D.J.A. Cockerill, J.A. Coughlan, K. Harder, S. Harper, J. Jackson, E. Olaiya, D. Petyt, B.C. Radburn-Smith, C.H. Shepherd-Themistocleous, I.R. Tomalin, W.J. Womersley

Imperial College, London, United Kingdom
R. Bainbridge, G. Ball, O. Buchmuller, D. Colling, N. Cripps, M. Cutajar, P. Dauncey, G. Davies, M. Della Negra, W. Ferguson, J. Fulcher, A. Gilbert, A. Guneratne Bryer, G. Hall, Z. Hatherell, J. Hays, G. Iles, M. Jarvis, G. Karapostoli, M. Kenzie, L. Lyons, A.-M. Magnan, J. Marrouche, B. Mathias, R. Nandi, J. Nash, A. Nikitenko[35], J. Pela, M. Pesaresi, K. Petridis, M. Pioppi[49], D.M. Raymond, S. Rogerson, A. Rose, C. Seez, P. Sharp[†], A. Sparrow, A. Tapper, M. Vazquez Acosta, T. Virdee, S. Wakefield, N. Wardle, T. Whyntie

Brunel University, Uxbridge, United Kingdom
M. Chadwick, J.E. Cole, P.R. Hobson, A. Khan, P. Kyberd, D. Leggat, D. Leslie, W. Martin, I.D. Reid, P. Symonds, L. Teodorescu, M. Turner

Baylor University, Waco, USA
J. Dittmann, K. Hatakeyama, A. Kasmi, H. Liu, T. Scarborough

The University of Alabama, Tuscaloosa, USA
O. Charaf, S.I. Cooper, C. Henderson, P. Rumerio

Boston University, Boston, USA
A. Avetisyan, T. Bose, C. Fantasia, A. Heister, P. Lawson, D. Lazic, J. Rohlf, D. Sperka, J. St. John, L. Sulak

Brown University, Providence, USA
J. Alimena, S. Bhattacharya, G. Christopher, D. Cutts, Z. Demiragli, A. Ferapontov, A. Garabedian, U. Heintz, G. Kukartsev, E. Laird, G. Landsberg, M. Luk, M. Narain, M. Segala, T. Sinthuprasith, T. Speer

University of California, Davis, Davis, USA
R. Breedon, G. Breto, M. Calderon De La Barca Sanchez, M. Caulfield, S. Chauhan, M. Chertok, J. Conway, R. Conway, P.T. Cox, J. Dolen, R. Erbacher, M. Gardner, R. Houtz, W. Ko, A. Kopecky, R. Lander, O. Mall, T. Miceli, R. Nelson, D. Pellett, F. Ricci-Tam, B. Rutherford, M. Searle, J. Smith, M. Squires, M. Tripathi, R. Yohay

University of California, Los Angeles, USA
V. Andreev, D. Cline, R. Cousins, J. Duris, S. Erhan, P. Everaerts, C. Farrell, M. Felcini, J. Hauser, M. Ignatenko, C. Jarvis, G. Rakness, P. Schlein[†], P. Traczyk, V. Valuev, M. Weber

University of California, Riverside, Riverside, USA
J. Babb, R. Clare, M.E. Dinardo, J. Ellison, J.W. Gary, F. Giordano, G. Hanson, H. Liu, O.R. Long, A. Luthra, H. Nguyen, S. Paramesvaran, J. Sturdy, S. Sumowidagdo, R. Wilken, S. Wimpenny

University of California, San Diego, La Jolla, USA
W. Andrews, J.G. Branson, G.B. Cerati, S. Cittolin, D. Evans, A. Holzner, R. Kelley, M. Lebourgeois, J. Letts, I. Macneill, B. Mangano, S. Padhi, C. Palmer, G. Petrucciani, M. Pieri, M. Sani, V. Sharma, S. Simon, E. Sudano, M. Tadel, Y. Tu, A. Vartak, S. Wasserbaech[50], F. Würthwein, A. Yagil, J. Yoo

University of California, Santa Barbara, Santa Barbara, USA
D. Barge, R. Bellan, C. Campagnari, M. D'Alfonso, T. Danielson, K. Flowers, P. Geffert, C. George, F. Golf, J. Incandela, C. Justus, P. Kalavase, D. Kovalskyi, V. Krutelyov, S. Lowette, R. Magaña Villalba, N. Mccoll, V. Pavlunin, J. Ribnik, J. Richman, R. Rossin, D. Stuart, W. To, C. West

California Institute of Technology, Pasadena, USA
A. Apresyan, A. Bornheim, J. Bunn, Y. Chen, E. Di Marco, J. Duarte, D. Kcira, Y. Ma, A. Mott, H.B. Newman, C. Rogan, M. Spiropulu, V. Timciuc, J. Veverka, R. Wilkinson, S. Xie, Y. Yang, R.Y. Zhu

Carnegie Mellon University, Pittsburgh, USA
V. Azzolini, A. Calamba, R. Carroll, T. Ferguson, Y. Iiyama, D.W. Jang, Y.F. Liu, M. Paulini, J. Russ, H. Vogel, I. Vorobiev

University of Colorado at Boulder, Boulder, USA
J.P. Cumalat, B.R. Drell, W.T. Ford, A. Gaz, E. Luiggi Lopez, U. Nauenberg, J.G. Smith, K. Stenson, K.A. Ulmer, S.R. Wagner

Cornell University, Ithaca, USA
J. Alexander, A. Chatterjee, N. Eggert, L.K. Gibbons, W. Hopkins, A. Khukhunaishvili, B. Kreis, N. Mirman, G. Nicolas Kaufman, J.R. Patterson, A. Ryd, E. Salvati, W. Sun, W.D. Teo, J. Thom, J. Thompson, J. Tucker, Y. Weng, L. Winstrom, P. Wittich

Fairfield University, Fairfield, USA
D. Winn

Fermi National Accelerator Laboratory, Batavia, USA
S. Abdullin, M. Albrow, J. Anderson, G. Apollinari, L.A.T. Bauerdick, A. Beretvas, J. Berryhill, P.C. Bhat, K. Burkett, J.N. Butler, V. Chetluru, H.W.K. Cheung, F. Chlebana, S. Cihangir,

V.D. Elvira, I. Fisk, J. Freeman, Y. Gao, E. Gottschalk, L. Gray, D. Green, O. Gutsche, R.M. Harris, J. Hirschauer, B. Hooberman, S. Jindariani, M. Johnson, U. Joshi, B. Klima, S. Kunori, S. Kwan, J. Linacre, D. Lincoln, R. Lipton, J. Lykken, K. Maeshima, J.M. Marraffino, V.I. Martinez Outschoorn, S. Maruyama, D. Mason, P. McBride, K. Mishra, S. Mrenna, Y. Musienko[51], C. Newman-Holmes, V. O'Dell, O. Prokofyev, E. Sexton-Kennedy, S. Sharma, W.J. Spalding, L. Spiegel, L. Taylor, S. Tkaczyk, N.V. Tran, L. Uplegger, E.W. Vaandering, R. Vidal, J. Whitmore, W. Wu, F. Yang, J.C. Yun

University of Florida, Gainesville, USA
D. Acosta, P. Avery, D. Bourilkov, M. Chen, T. Cheng, S. Das, M. De Gruttola, G.P. Di Giovanni, D. Dobur, A. Drozdetskiy, R.D. Field, M. Fisher, Y. Fu, I.K. Furic, J. Hugon, B. Kim, J. Konigsberg, A. Korytov, A. Kropivnitskaya, T. Kypreos, J.F. Low, K. Matchev, P. Milenovic[52], G. Mitselmakher, L. Muniz, R. Remington, A. Rinkevicius, N. Skhirtladze, M. Snowball, J. Yelton, M. Zakaria

Florida International University, Miami, USA
V. Gaultney, S. Hewamanage, L.M. Lebolo, S. Linn, P. Markowitz, G. Martinez, J.L. Rodriguez

Florida State University, Tallahassee, USA
T. Adams, A. Askew, J. Bochenek, J. Chen, B. Diamond, S.V. Gleyzer, J. Haas, S. Hagopian, V. Hagopian, K.F. Johnson, H. Prosper, V. Veeraraghavan, M. Weinberg

Florida Institute of Technology, Melbourne, USA
M.M. Baarmand, B. Dorney, M. Hohlmann, H. Kalakhety, F. Yumiceva

University of Illinois at Chicago (UIC), Chicago, USA
M.R. Adams, L. Apanasevich, V.E. Bazterra, R.R. Betts, I. Bucinskaite, J. Callner, R. Cavanaugh, O. Evdokimov, L. Gauthier, C.E. Gerber, D.J. Hofman, S. Khalatyan, P. Kurt, F. Lacroix, C. O'Brien, C. Silkworth, D. Strom, P. Turner, N. Varelas

The University of Iowa, Iowa City, USA
U. Akgun, E.A. Albayrak, B. Bilki[53], W. Clarida, K. Dilsiz, F. Duru, S. Griffiths, J.-P. Merlo, H. Mermerkaya[54], A. Mestvirishvili, A. Moeller, J. Nachtman, C.R. Newsom, H. Ogul, Y. Onel, F. Ozok[46], S. Sen, P. Tan, E. Tiras, J. Wetzel, T. Yetkin, K. Yi

Johns Hopkins University, Baltimore, USA
B.A. Barnett, B. Blumenfeld, S. Bolognesi, D. Fehling, G. Giurgiu, A.V. Gritsan, G. Hu, P. Maksimovic, M. Swartz, A. Whitbeck

The University of Kansas, Lawrence, USA
P. Baringer, A. Bean, G. Benelli, R.P. Kenny Iii, M. Murray, D. Noonan, S. Sanders, R. Stringer, J.S. Wood

Kansas State University, Manhattan, USA
A.F. Barfuss, I. Chakaberia, A. Ivanov, S. Khalil, M. Makouski, Y. Maravin, S. Shrestha, I. Svintradze

Lawrence Livermore National Laboratory, Livermore, USA
J. Gronberg, D. Lange, F. Rebassoo, D. Wright

University of Maryland, College Park, USA
A. Baden, B. Calvert, S.C. Eno, J.A. Gomez, N.J. Hadley, R.G. Kellogg, T. Kolberg, Y. Lu, M. Marionneau, A.C. Mignerey, K. Pedro, A. Peterman, A. Skuja, J. Temple, M.B. Tonjes, S.C. Tonwar

Massachusetts Institute of Technology, Cambridge, USA
A. Apyan, G. Bauer, W. Busza, E. Butz, I.A. Cali, M. Chan, V. Dutta, G. Gomez Ceballos, M. Goncharov, Y. Kim, M. Klute, A. Levin, P.D. Luckey, T. Ma, S. Nahn, C. Paus, D. Ralph, C. Roland, G. Roland, G.S.F. Stephans, F. Stöckli, K. Sumorok, K. Sung, D. Velicanu, R. Wolf, B. Wyslouch, M. Yang, Y. Yilmaz, A.S. Yoon, M. Zanetti, V. Zhukova

University of Minnesota, Minneapolis, USA
B. Dahmes, A. De Benedetti, G. Franzoni, A. Gude, J. Haupt, S.C. Kao, K. Klapoetke, Y. Kubota, J. Mans, N. Pastika, R. Rusack, M. Sasseville, A. Singovsky, N. Tambe, J. Turkewitz

University of Mississippi, Oxford, USA
L.M. Cremaldi, R. Kroeger, L. Perera, R. Rahmat, D.A. Sanders, D. Summers

University of Nebraska-Lincoln, Lincoln, USA
E. Avdeeva, K. Bloom, S. Bose, D.R. Claes, A. Dominguez, M. Eads, J. Keller, I. Kravchenko, J. Lazo-Flores, S. Malik, G.R. Snow

State University of New York at Buffalo, Buffalo, USA
A. Godshalk, I. Iashvili, S. Jain, A. Kharchilava, A. Kumar, S. Rappoccio, Z. Wan

Northeastern University, Boston, USA
G. Alverson, E. Barberis, D. Baumgartel, M. Chasco, J. Haley, D. Nash, T. Orimoto, D. Trocino, D. Wood, J. Zhang

Northwestern University, Evanston, USA
A. Anastassov, K.A. Hahn, A. Kubik, L. Lusito, N. Mucia, N. Odell, B. Pollack, A. Pozdnyakov, M. Schmitt, S. Stoynev, M. Velasco, S. Won

University of Notre Dame, Notre Dame, USA
D. Berry, A. Brinkerhoff, K.M. Chan, M. Hildreth, C. Jessop, D.J. Karmgard, J. Kolb, K. Lannon, W. Luo, S. Lynch, N. Marinelli, D.M. Morse, T. Pearson, M. Planer, R. Ruchti, J. Slaunwhite, N. Valls, M. Wayne, M. Wolf

The Ohio State University, Columbus, USA
L. Antonelli, B. Bylsma, L.S. Durkin, C. Hill, R. Hughes, K. Kotov, T.Y. Ling, D. Puigh, M. Rodenburg, G. Smith, J. Timcheck, C. Vuosalo, G. Williams, B.L. Winer, H. Wolfe

Princeton University, Princeton, USA
E. Berry, P. Elmer, V. Halyo, P. Hebda, J. Hegeman, A. Hunt, P. Jindal, S.A. Koay, D. Lopes Pegna, P. Lujan, D. Marlow, T. Medvedeva, M. Mooney, J. Olsen, P. Piroué, X. Quan, A. Raval, H. Saka, D. Stickland, C. Tully, J.S. Werner, S.C. Zenz, A. Zuranski

University of Puerto Rico, Mayaguez, USA
E. Brownson, A. Lopez, H. Mendez, J.E. Ramirez Vargas

Purdue University, West Lafayette, USA
E. Alagoz, D. Benedetti, G. Bolla, D. Bortoletto, M. De Mattia, A. Everett, Z. Hu, M. Jones, O. Koybasi, M. Kress, N. Leonardo, V. Maroussov, P. Merkel, D.H. Miller, N. Neumeister, I. Shipsey, D. Silvers, A. Svyatkovskiy, M. Vidal Marono, H.D. Yoo, J. Zablocki, Y. Zheng

Purdue University Calumet, Hammond, USA
S. Guragain, N. Parashar

Rice University, Houston, USA
A. Adair, B. Akgun, K.M. Ecklund, F.J.M. Geurts, W. Li, B.P. Padley, R. Redjimi, J. Roberts, J. Zabel

University of Rochester, Rochester, USA
B. Betchart, A. Bodek, R. Covarelli, P. de Barbaro, R. Demina, Y. Eshaq, T. Ferbel, A. Garcia-Bellido, P. Goldenzweig, J. Han, A. Harel, D.C. Miner, G. Petrillo, D. Vishnevskiy, M. Zielinski

The Rockefeller University, New York, USA
A. Bhatti, R. Ciesielski, L. Demortier, K. Goulianos, G. Lungu, S. Malik, C. Mesropian

Rutgers, The State University of New Jersey, Piscataway, USA
S. Arora, A. Barker, J.P. Chou, C. Contreras-Campana, E. Contreras-Campana, D. Duggan, D. Ferencek, Y. Gershtein, R. Gray, E. Halkiadakis, D. Hidas, A. Lath, S. Panwalkar, M. Park, R. Patel, V. Rekovic, J. Robles, K. Rose, S. Salur, S. Schnetzer, C. Seitz, S. Somalwar, R. Stone, M. Walker

University of Tennessee, Knoxville, USA
G. Cerizza, M. Hollingsworth, S. Spanier, Z.C. Yang, A. York

Texas A&M University, College Station, USA
R. Eusebi, W. Flanagan, J. Gilmore, T. Kamon[55], V. Khotilovich, R. Montalvo, I. Osipenkov, Y. Pakhotin, A. Perloff, J. Roe, A. Safonov, T. Sakuma, I. Suarez, A. Tatarinov, D. Toback

Texas Tech University, Lubbock, USA
N. Akchurin, J. Damgov, C. Dragoiu, P.R. Dudero, C. Jeong, K. Kovitanggoon, S.W. Lee, T. Libeiro, I. Volobouev

Vanderbilt University, Nashville, USA
E. Appelt, A.G. Delannoy, S. Greene, A. Gurrola, W. Johns, C. Maguire, Y. Mao, A. Melo, M. Sharma, P. Sheldon, B. Snook, S. Tuo, J. Velkovska

University of Virginia, Charlottesville, USA
M.W. Arenton, M. Balazs, S. Boutle, B. Cox, B. Francis, J. Goodell, R. Hirosky, A. Ledovskoy, C. Lin, C. Neu, J. Wood

Wayne State University, Detroit, USA
S. Gollapinni, R. Harr, P.E. Karchin, C. Kottachchi Kankanamge Don, P. Lamichhane, A. Sakharov

University of Wisconsin, Madison, USA
M. Anderson, D.A. Belknap, L. Borrello, D. Carlsmith, M. Cepeda, S. Dasu, E. Friis, K.S. Grogg, M. Grothe, R. Hall-Wilton, M. Herndon, A. Hervé, P. Klabbers, J. Klukas, A. Lanaro, C. Lazaridis, R. Loveless, A. Mohapatra, M.U. Mozer, I. Ojalvo, G.A. Pierro, I. Ross, A. Savin, W.H. Smith, J. Swanson

†: Deceased
1: Also at Vienna University of Technology, Vienna, Austria
2: Also at CERN, European Organization for Nuclear Research, Geneva, Switzerland
3: Also at National Institute of Chemical Physics and Biophysics, Tallinn, Estonia
4: Also at Skobeltsyn Institute of Nuclear Physics, Lomonosov Moscow State University, Moscow, Russia
5: Also at Universidade Estadual de Campinas, Campinas, Brazil
6: Also at California Institute of Technology, Pasadena, USA
7: Also at Laboratoire Leprince-Ringuet, Ecole Polytechnique, IN2P3-CNRS, Palaiseau, France
8: Also at Suez Canal University, Suez, Egypt
9: Also at Cairo University, Cairo, Egypt
10: Also at Fayoum University, El-Fayoum, Egypt

11: Also at British University in Egypt, Cairo, Egypt
12: Now at Ain Shams University, Cairo, Egypt
13: Also at National Centre for Nuclear Research, Swierk, Poland
14: Also at Université de Haute Alsace, Mulhouse, France
15: Also at Joint Institute for Nuclear Research, Dubna, Russia
16: Also at Brandenburg University of Technology, Cottbus, Germany
17: Also at The University of Kansas, Lawrence, USA
18: Also at Institute of Nuclear Research ATOMKI, Debrecen, Hungary
19: Also at Eötvös Loránd University, Budapest, Hungary
20: Also at Tata Institute of Fundamental Research - HECR, Mumbai, India
21: Now at King Abdulaziz University, Jeddah, Saudi Arabia
22: Also at University of Visva-Bharati, Santiniketan, India
23: Also at Sharif University of Technology, Tehran, Iran
24: Also at Isfahan University of Technology, Isfahan, Iran
25: Also at Plasma Physics Research Center, Science and Research Branch, Islamic Azad University, Tehran, Iran
26: Also at Facoltà Ingegneria, Università di Roma, Roma, Italy
27: Also at Laboratori Nazionali di Legnaro dell' INFN, Legnaro, Italy
28: Also at Università degli Studi di Siena, Siena, Italy
29: Also at Faculty of Physics, University of Belgrade, Belgrade, Serbia
30: Also at Scuola Normale e Sezione dell'INFN, Pisa, Italy
31: Also at INFN Sezione di Roma, Roma, Italy
32: Also at University of Athens, Athens, Greece
33: Also at Rutherford Appleton Laboratory, Didcot, United Kingdom
34: Also at Paul Scherrer Institut, Villigen, Switzerland
35: Also at Institute for Theoretical and Experimental Physics, Moscow, Russia
36: Also at Albert Einstein Center for Fundamental Physics, Bern, Switzerland
37: Also at Gaziosmanpasa University, Tokat, Turkey
38: Also at Adiyaman University, Adiyaman, Turkey
39: Also at The University of Iowa, Iowa City, USA
40: Also at Mersin University, Mersin, Turkey
41: Also at Izmir Institute of Technology, Izmir, Turkey
42: Also at Ozyegin University, Istanbul, Turkey
43: Also at Kafkas University, Kars, Turkey
44: Also at Suleyman Demirel University, Isparta, Turkey
45: Also at Ege University, Izmir, Turkey
46: Also at Mimar Sinan University, Istanbul, Istanbul, Turkey
47: Also at Kahramanmaras Sütcü Imam University, Kahramanmaras, Turkey
48: Also at School of Physics and Astronomy, University of Southampton, Southampton, United Kingdom
49: Also at INFN Sezione di Perugia; Università di Perugia, Perugia, Italy
50: Also at Utah Valley University, Orem, USA
51: Also at Institute for Nuclear Research, Moscow, Russia
52: Also at University of Belgrade, Faculty of Physics and Vinca Institute of Nuclear Sciences, Belgrade, Serbia
53: Also at Argonne National Laboratory, Argonne, USA
54: Also at Erzincan University, Erzincan, Turkey
55: Also at Kyungpook National University, Daegu, Korea